Fractography analysis of tool samples used for cold forging

Dahl, K.V.

Publication date:
2002

Document Version
Publisher's PDF, also known as Version of record

Risø-R-1359(EN)

Fractography analysis of tool samples used for cold forging

Kristian Vinter Dahl

Risø National Laboratory, Roskilde
August 2002

Abstract Three fractured tool dies used for industrial cold forging have been investigated using light optical microscopy and scanning electron microscopy. Two of the specimens were produced using the traditional Böhler P/M steel grade s790, while the last specimen was a third generation P/M steel produced using new technology developed by Böhler. All three steels have the same nominal composition of alloying elements.

The failure in both types of material occurs as a crack formation at a notch inside of the tool. Generally the cold forging dies constructed in third generation steels have a longer lifetime than the ones constructed in traditional steel, which is connected to differences in microstructure. Focus has been put on differences in the size and distribution of carbides. It is found that the third generation steel contains smaller and more finely dispersed carbides and has an increased resistance towards abrasive wear compared with the traditional P/M steel.

It was discovered that a cleaning agent (Alconox) frequently used for the cleaning of fracture surfaces introduced changes to the surface morphology. Therefore work was put into finding out exactly how this influenced the specimens looked upon. The result of this work is included as a separate part of this document (Appendix A).

ISBN 87-550-3102-1
ISBN 87-550-3104-8 (Internet)

ISSN 0106-2840

Print: Pitney Bowes Management Services Denmark A/S, 2002

Contents

1 Introduction

1.1 Cold forging

Cold forging is a process used for large-scale production of small metal components. For instance cold forging is a much-used process in the automotive industry for production of axles and valve houses and other intricate parts.

In comparison to traditional machining the use of cold forging is profitable since it offers a more automated process and a lot less material waste, because of the possibility of producing net shape or near net shape products. Figure 1-1 shows examples of parts produced by cold forging.

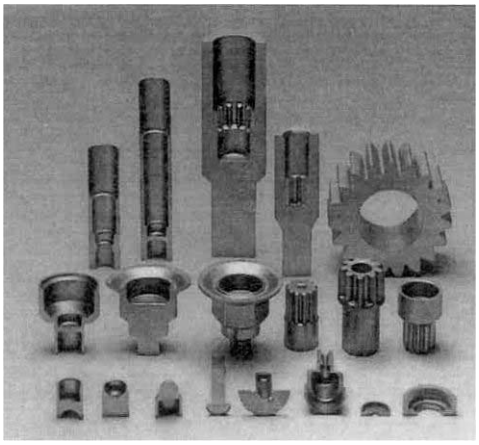

Figure 1-1 Examples of cold forged steel products produced at Danfoss A/S [1].

In cold forging the billet material is at near room temperature and therefore very high mechanical loads are needed to form the material. This means that during a production run the tool is subjected to repeat loadings under very high stresses. These stresses can often be very close to or even exceed the critical yield stress at notches and bends and other stress-concentrating details in the tool. This results in local critical plastic strains, which lead to dimensional changes and sudden fracture of the tool [2]. In order to minimize the risk of these effects and to prolong the lifetime of the tool a lot of care is put into designing through finite element modelling (FEM) (See for example [3]), material selection, heat treatment, surface treatment etc.

Prestressing

A way of increasing tool life significantly is by compressive prestressing of the tool. This is traditionally done by fitting a die into one or multiple stress rings by shrinking, however the die life can be further increased by using the strip-winding technology invented by STRECON A/S. Figure 1-2 illustrates a conventional set up using stress rings and a set up using STRECON® technology. Strip-winding containers can effectively improve the die lives by typically a factor of 3 to 10 depending on the exact application [4].

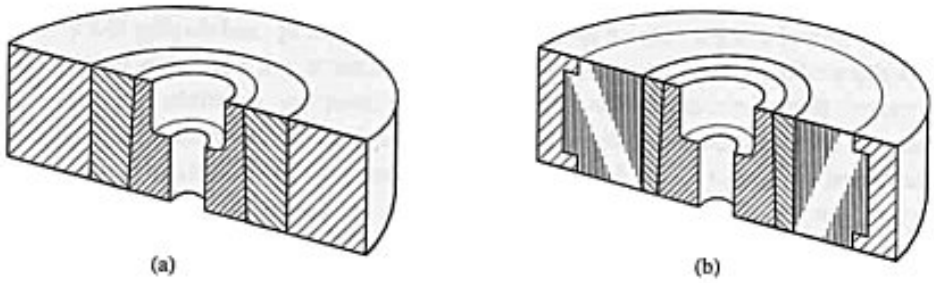

Figure 1-2 (a) Conventional stress rings. (b) Strip-wound container [1].

The STRECON® strip-wound containers are manufactured by winding a thin strip of high-strength steel around a core of high stiffness material such as cemented carbide, as can be seen in Figure 1-3. By varying the winding tension from layer to layer an optimum stress distribution in the die can be obtained [1], whereby damaging cyclic-plastic strain is reduced in the most exposed parts of the die geometry.

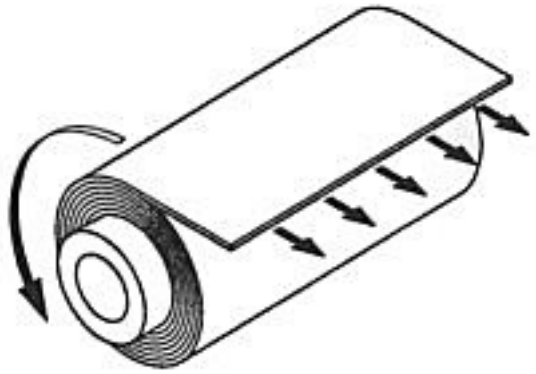

Figure 1-3 Winding principle of STRECON® prestressed container [1].

In this way a strip-wound set up would correspond to a conventional set up with several hundreds of stress rings. Therefore it is possible to operate with higher internal pressures and stresses in the die before the material deforms plastically and failure occurs. Thus the use of the strip-wound containers increases the die-life whereby the manufacturing cost is lowered and also allows the production of parts with a complicated geometry. The reduction of radial deflections of the die during the cold forging process improves conditions for production of net shape or near net shape parts.

High-speed tool steels

Typical materials used for cold forging tools are P/M (powder metallurgical) high-speed tool steels like for example the classic Vanadis 23 delivered by Uddeholm Tooling AB, Sweden, which conforms to the AISI M3:2 standard. Other materials that can be used are cemented carbides like tungsten carbide.

High-speed tool steels are complex iron-base alloys with a matrix of tempered martensite and with additions of chromium, vanadium, molybdenum, or tungsten or combinations thereof and in some steels large substantial amounts of cobalt. The content of carbon and other alloys are balanced at levels to give high wear resistance, good toughness and high attainable hardening response.

The high-speed tool steels are classified according to the AISI system. Steels that have tungsten as one of their main alloying elements are designated with a T and those that have molybdenum as one of their primary alloying elements are designated with an M. After the M or the T follows a number that is only used to distinguish the different tool steels from each other. The number does not tell anything about amount of alloying elements or other characteristics.

Heat treatment

The final microstructure of high-speed tool steels consists of tempered martensite containing finely dispersed carbides. Normally the tool steel is delivered in fully annealed condition and a three-step heat treatment is applied. Each step introduces new changes to the microstructure and has influence on the final properties of the tool steel. The three steps are: Austenitizing, quenching and tempering.

The general procedure for the heat treatment of tool steels is shown in Figure 1-4.

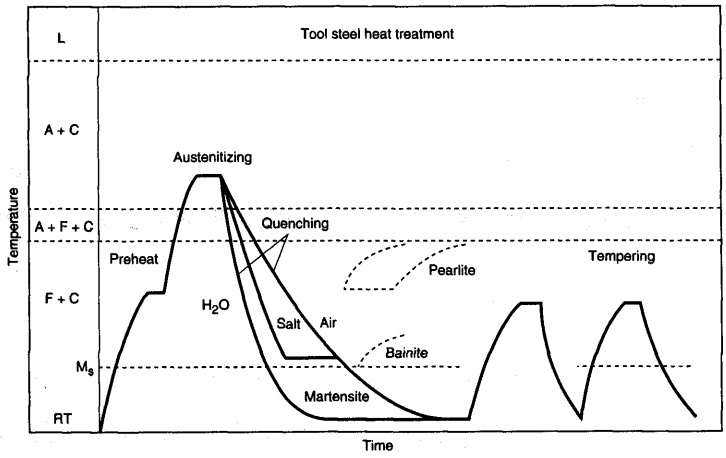

Figure 1-4 Schematic diagram of tool steel heat treatment steps for final hardening [5].

Austenitizing is done in the austenite and carbon area of the phase diagram. The process temperature and holding time is chosen so as to obtain a homogeneous microstructure while avoiding excessive grain-growth. The chosen austenitizing temperature is decisive for the amount of undissolved carbides (primary carbides) and the amount of carbon and alloying elements in the austenite phase, whereby final carbon volume fraction, hardenability, retained austenite content, and secondary hardening potential are all influenced.

The quenching is a diffusionless transformation of austenite into martensite (the martensite has same composition as the original austenite). The cooling rate must be high enough to ensure that the diffusion of carbon and other alloying elements are avoided but not so high that dimensional changes or heat cracks are introduced.

The final step, tempering, is performed in order to increase the toughness and fracture resistance of the tool steel. The martensite present in the quenched condition is too brittle to be of use in tool application. The tempering takes place in

the ferrite and carbon area of the phase diagram (~500-600˚C) and often two or three tempering steps of duration of approximately one hour each are applied. During the tempering the highly alloyed tool steels also experience secondary hardening due to the precipitation of minute secondary carbides coherent with the matrix.

Effect of alloying elements [6],[7]

The various alloying elements added all have a unique effect on the properties of the produced high-speed steel. The effects of the most important alloying elements are shortly discussed in the following.

Carbon is the most important element and the amount added is very closely controlled since even a small change in carbon content can have a large impact on material properties. With increasing carbon content the working hardness rises, the elevated temperature hardness rises, and the number of complex, stable carbides that contribute to the wear resistance increases. The carbides observed in high-speed steels are:

- M_6C, tungsten- or molybdenum carbide-rich fcc carbide of the composition ranges Fe_3W_3C to Fe_4W_2C in tungsten alloys and Fe_3Mo_3C to Fe_4Mo_2C in molybdenum alloys. The carbide is capable of dissolving some chromium, vanadium and cobalt.
- $M_{23}C_6$, chromium-rich fcc carbide ($Cr_{23}C_6$) capable of dissolving iron, tungsten, molybdenum and vanadium.
- MC, vanadium-rich fcc carbide of composition range VC to V_4C_3 capable of dissolving limited amounts of tungsten, molybdenum, chromium and iron.
- M_2C, tungsten- or molybdenum-rich hcp carbide that is only observed as a transition phase formed during the tempering of high-speed steels.

The high-speed tool steels have very large fractions of carbides, which can be seen in Figure 1-5.

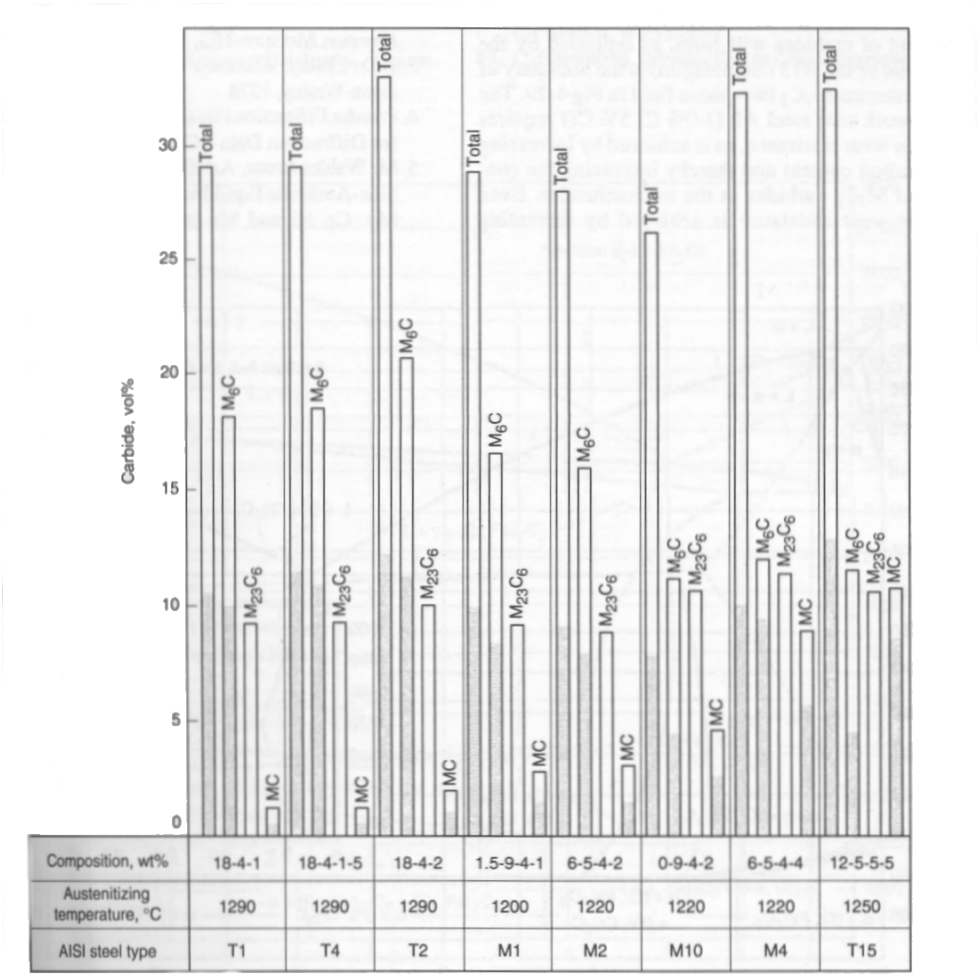

Composition, wt%	18-4-1	18-4-1-5	18-4-2	1.5-9-4-1	6-5-4-2	0-9-4-2	6-5-4-4	12-5-5-5
Austenitizing temperature, °C	1290	1290	1290	1200	1220	1220	1220	1250
AISI steel type	T1	T4	T2	M1	M2	M10	M4	T15

Figure 1-5 Volume percentages of carbides in high-speed steels as-annealed (white bars) and after austenitizing for hardening (grey bars). Compositions of T high-speed steels are given in weight percent as W-Cr-V-Co and of M high-speed steels as W-Mo-Cr-V [6].

The amount of carbon in solid solution in the matrix decides whether the martensite formed during the heat treatment is of lath or plate-type. When the C-content of the matrix is below approximately 0,4 wt% lath-type martensite is formed and at higher C-contents plate-type martensite is formed [8]. Which type is preferred depends on whether toughness (lath-type) or resistance against abrasive wear (plate-type) is desired [6].

Chromium is important for the hardenability; usually a content of about 4 wt% is used, because this gives the best compromise between toughness and hardness.

Tungsten forms very hard complex carbides, which contribute significantly to the wear resistance of the steel. Tungsten also improves hot hardness, causes secondary hardening, and imparts marked resistance to hardening.

Molybdenum forms the same type of carbides as tungsten does, and therefore tungsten can be substituted by molybdenum. Molybdenum has approximately half the atomic weight of tungsten, and therefore two parts of tungsten by weight can be substituted by one part of molybdenum. M-type steels generally have a higher toughness compared to the T-type steels and a slightly lower hot

hardness. Addition of tungsten to the M-type steels compensate for this last effect. The molybdenum steels are generally cheaper and are therefore more widely used.

Vanadium forms very hard stable VC carbides, which dramatically increase the wear resistance. When properly balanced by the carbon additions the effect of vanadium on the toughness of the steel is relatively little.

Cobalt is mainly used to increase the hot hardness. The heat-treating temperature rises because cobalt elevates the melting point, and it also slightly increases the brittleness of the high-speed steel.

Powder metallurgy

Powder metallurgy (P/M) is a widely used method for production of most high-carbon, high-alloy tool steels, and it has several advantages compared to traditional ingot casting. The relatively slow cooling rate of a conventional static cast ingot makes it hard to obtain a satisfyingly fine carbide structure and a uniform dispersion of the carbides. This can result in nonuniform and excessive grain growth, nonuniform response to heat treatment, poor transverse properties and low toughness. P/M provides an efficient way to overcome these problems.

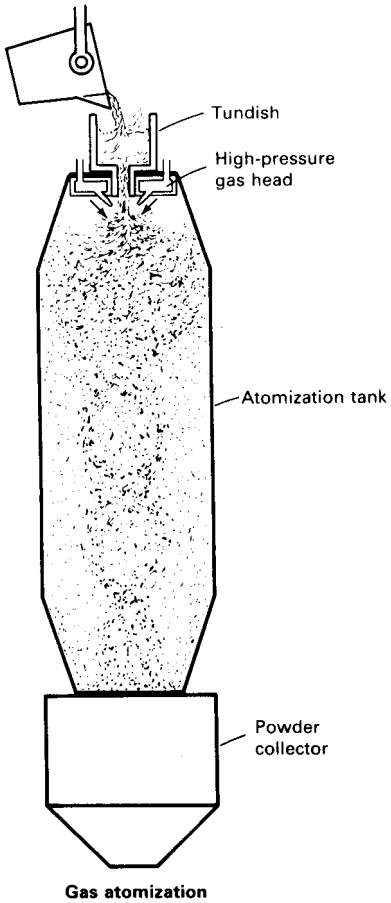

The gas atomization is the most widely used process for the production of P/M tool steels. The process is illustrated on Figure 1-6. Molten metal is poured through a small diameter nozzle into jets of high-pressure gas (nitrogen or argon) that break the stream into many small droplets. Each droplet can be considered as a mini-ingot that solidifies on it's way towards the bottom of the chamber.

The resulting component cannot be produced by the traditional press- and sinter technique because the powder's highly spherical nature results in an insufficient green strength. Instead the material is hot isostatically pressed (HIPed) in a vacuum container. In this way full density is achieved.

Figure 1-6 Schematic diagram of the gas atomization process [5].

Figure 1-7 shows traditional wrought steel and a P/M steel of the same composition. It is obvious that the P/M process provides a much more homogeneous structure and a much finer dispersion of the carbides. This is especially important when the material is to be used as a tool for cold forging, since the coarse carbides in the wrought steel can act as crack initiation sites.

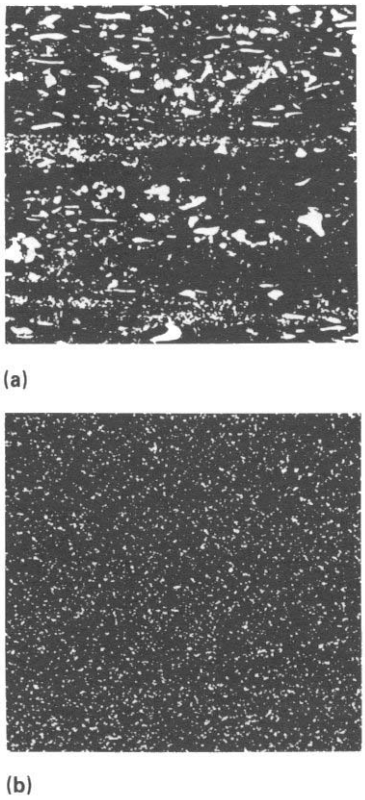

The small and finely dispersed carbides of the P/M structure improves the resistance against fracture and thereby fatigue cracking [6], and also makes it possible to use higher alloy contents compared to the conventional wrought materials.

Figure 1-7 Microstructure of T15 tool steel. (a) Wrought. (b) P/M manufactured [6].

Third generation P/M steels

The third generation P/M steels are the result of new technology developed by Böhler. The difference from the traditional steels lies in the method used for producing the powder used in the P/M process and possibly also in the heat treatment strategy. The exact procedure is only known to people within the Böhler company. It is claimed that this new production method offers a more homogeneous microstructure with smaller and more finely dispersed carbides and a higher purity compared with the traditional P/M steels.

Fracture of high-speed steels

The high-speed steels used for cold forging dies are subject to cyclic mechanical load and to fluctuations in temperature during industrial production, as a result of this cracking due to fatigue is a big problem.

In recent scientific work [9] it has been found that cracking of carbides at loads corresponding to a lower stress value than the yield stress of the steel has a large effect on the initiation of micro cracks and therefore on the fatigue properties of high strength tool steels.

Fatigue crack propagation is divided in to three stages. During stage I cracks are initiated and microstructure controlled crack propagation takes place. When a crack or defect reaches a certain critical size it becomes nearly independent of the microstructure and stage II is entered. In stage II steady-state crack propagation occurs following the Paris-Erdogan law:

$$\frac{da}{dN} = C(\Delta K)^m$$

where $\frac{da}{dN}$ is the crack growth per cycle, C and m are constants for a particular material and ΔK is the stress intensity factor, which is a function of applied load, specimen geometry and crack length.

In stage III catastrophic fast fracture occurs. Figure 1-8 gives an overview of the three stages.

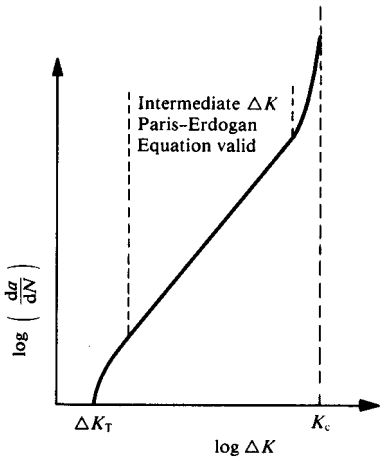

Figure 1-8 Relationship between fatigue crack growth and the stress intensity factor K. K_T is the threshold stress intensity factor (below this value crack growth is negligible) and K_c is the critical stress intensity factor. The three different stages of crack growth are separated by dotted lines [10].

Figure 1-9 shows the initiation of a fatigue crack in a test specimen made of P/M high-speed steel conforming to the AISI M3:2 standard (Vanadis 23 from Uddeholm Tooling AB). On Figure 1-9 (b) several ratchet lines can be observed, these marks indicate that there are multiple fatigue crack origins that grow and link up. The ratchet lines are steplike junctions between adjacent fatigue cracks. Ratchet lines indicate a homogenous material since the criteria for fracture crack initiation is met at multiple positions in the material at the same time. Figure (c) and (d) show that in the immediate area of crack initiation several cracked carbides are present but deeper in the material the crack propagates by cleavage of the matrix (approximately independent of the microstructure) and the amount of fractured carbides are significantly lower.

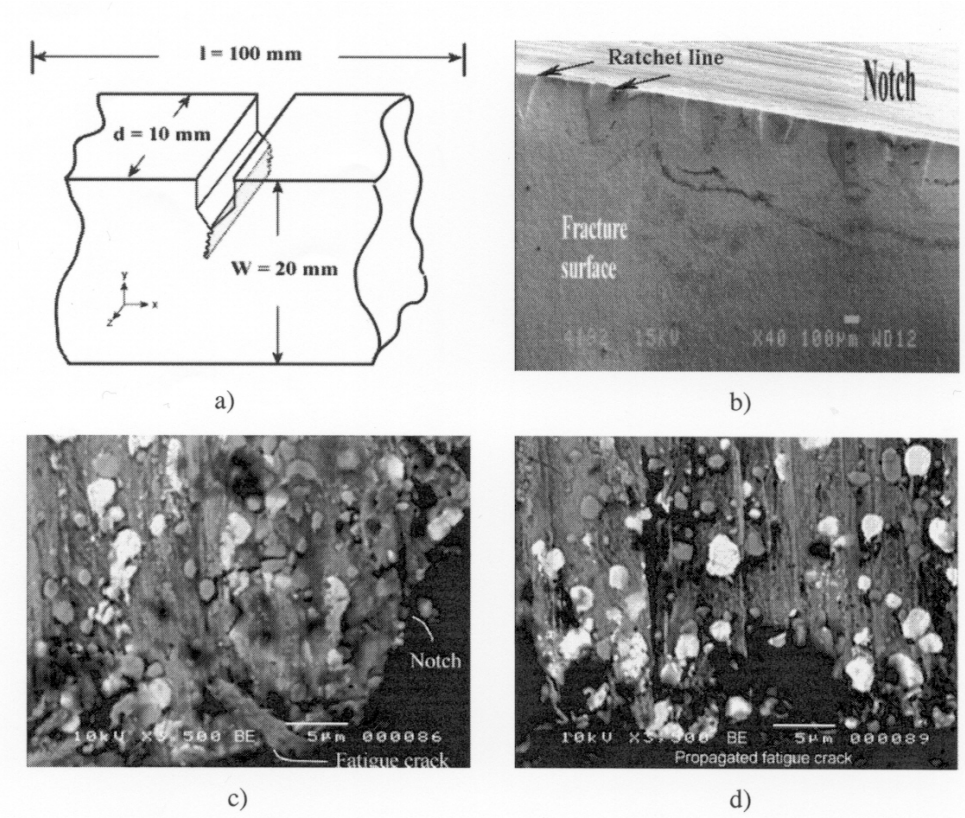

Figure 1-9 Single edge notch bend specimen after fatigue crack growth. (a) Sketch of the specimen with notch and fatigue crack. (b) Fracture surface (SEM SE contrast). (c) Surface in vicinity of the crack (normal parallel to the z-axis shown in (a)) (SEM BE contrast). (d) Same as (c) but 100 µm away from the notch root [9].

When final fracture occurs (stage III) the final fracture mode depends on the material and the service conditions. Figure 1-10 Shows the two fundamentally different fracture modes; ductile and brittle on tensile test specimens.

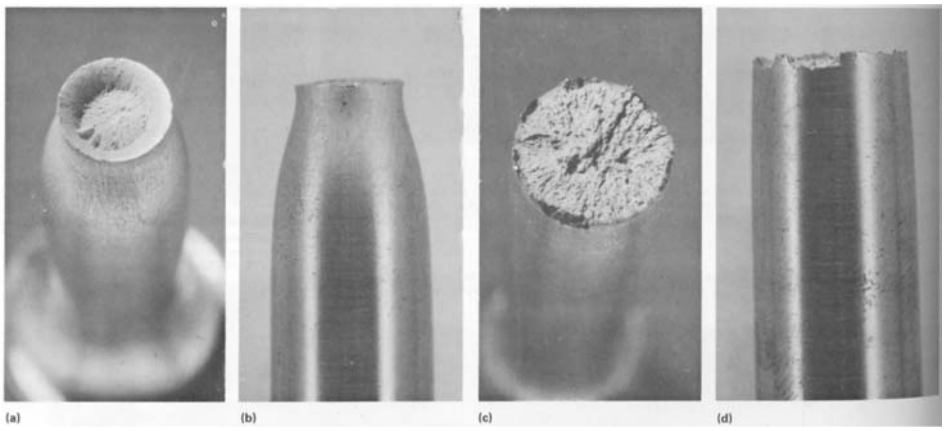

Figure 1-10 Macroscopic appearance of ductile (a) and brittle (b) tensile fractures [11].

The high-speed steels used for cold forging dies are brittle materials.

2 Methods of analysis

2.1 Light optical microscopy (LOM) (Metallurgical microscope) [12]

Light optical microscopy is usually the first step when investigating the microstructure of a metal. Using the metallurgical microscope on prepared surfaces allows the probing of the internal structure of materials. The LOM offers the possibility of direct visual observation of microstructural features of sizes below the resolving power of the human eye (0,1 mm). Information about morphology, size, colour, transparency and optical properties can be obtained.

The LOM has a maximum resolving power of approximately 0,2 μm when using white light and this can be further improved by using monochromatic light to a theoretical maximum of 0,150 μm.

The resolution r of the microscope depends on the wavelength λ of the used light and on the numerical aperture NA of the objective and the condenser, which is a measure of the light-gathering ability of the of the objective, or light-providing ability of the condenser.

$$r = \frac{\lambda}{2NA}$$

The numerical aperture depends on the refractive index of the medium between the specimen and the front lens. The maximum theoretical numerical aperture for a dry system is 1,0 (0,95 can be obtained practically), but by the use of oil-immersion objectives and condensers a practical numerical aperture of approximately 1,4 can be reached.

The maximum useful magnification in a modern LOM is 1400x. Many microscopes provide larger magnifications i.e. up to 5000x, but this is “empty” magnification. No further information is revealed beyond that observed at 1400x, because the microscope has reached the limit of its resolving power.

2.2 Scanning electron microscopy (SEM)

The SEM is used to investigate the surface or near surface area of bulk specimens. A schematic diagram showing the general components of the SEM can be seen on Figure 2-1

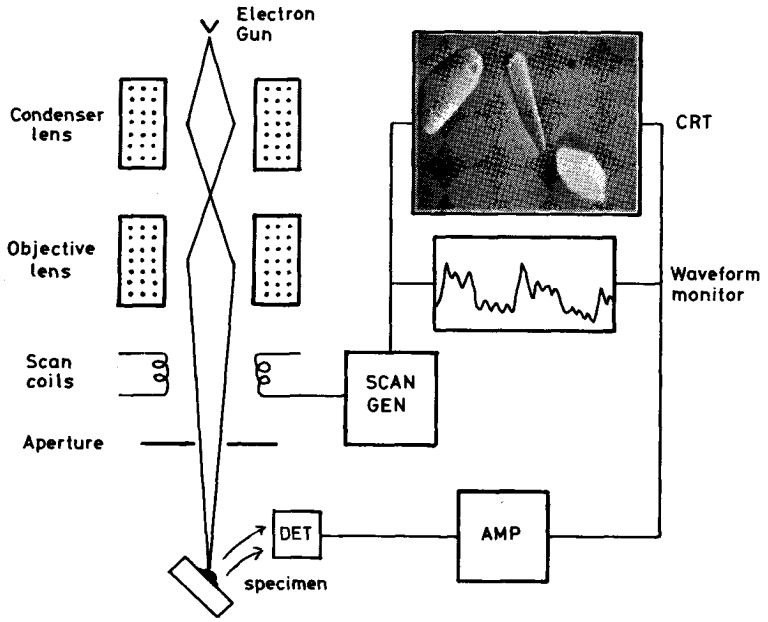

Figure 2-1 Schematic diagram of a SEM [13].

In the SEM an electron beam with electron energies about 2keV-40keV is scanned across the specimen surface by a system of scan coils (See Figure 2-1). The interaction between electron beam and specimen provides several signals, which can be used for imaging or obtaining chemical information. The information obtained depends on which signal is detected. The typical SEM is fitted with detectors for secondary- and backscattered electrons for imaging purposes, and is also frequently equipped with an energy dispersive spectrometer (EDS) that detects X-rays for chemical analysis.

Figure 2-2 shows the interaction volume of the electron beam and the regions from which the secondary electrons, backscattered electrons and X-rays may be detected.

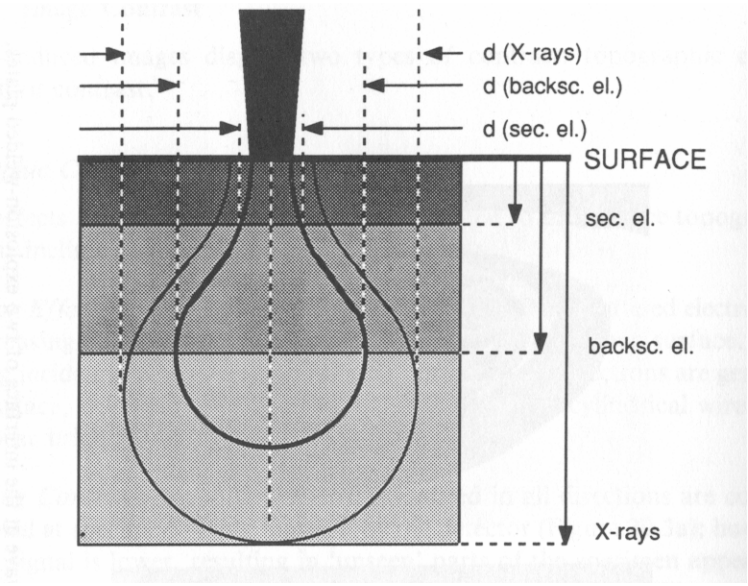

Figure 2-2 Interaction volume and the regions from which the different signals can be obtained [13].

The interaction volume is the region into which the electrons penetrate the specimen. Throughout this area radiations are generated as the result of inelastic scattering.

Secondary electrons

Secondary electrons are generated by primary electrons entering the specimen, by the escaping backscattered electrons and possibly by other secondary electrons of a higher energy as a result of inelastic collisions. Because of this the secondary electron energy spectrum is very broad and cannot directly be related to the chemical composition of the specimen. The secondary electrons are very numerous (the electron yield can be as high as 1 secondary electron per primary electron entering the specimen [13]) and as can be seen from Figure 2-2 come from a relatively little sample volume compared to the other radiations (sampling depth of a few angstroms). This means that the secondary electrons have an excellent signal to noise ratio and that they are capable of giving a better spatial resolution than the other signals obtained.

Backscattered electrons

Some of the primary electrons may leave the surface without having lost all of their energy, and they are most likely to do so while they still have a large fraction of their incident energy. These backscattered electrons are not as abundant as the secondary electrons and they originate from a larger volume of the specimen than the secondary electrons. As a result of this the signal to noise ratio and spatial resolution are not nearly as good as for the secondary electrons. In contrast to secondary electrons, the yield of backscattered electrons depends largely on atomic number, and therefore the backscattered electrons cannot only be used to provide topographic information about the test-specimen, but it is also possible to obtain information about composition.

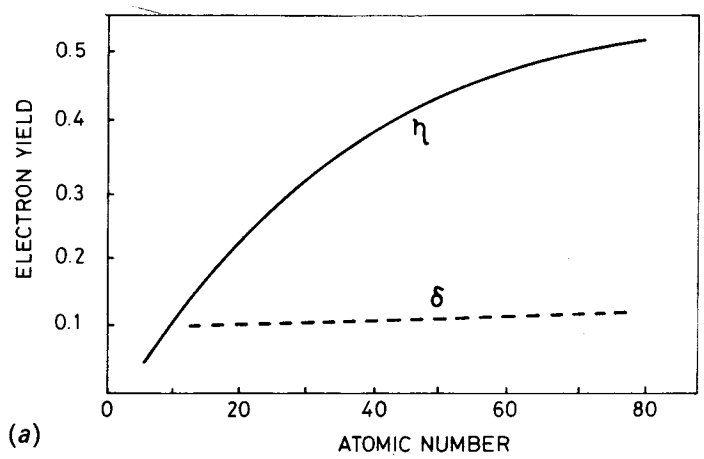

Figure 2-3 Electron yield of backscattered (η) and secondary electrons (δ) as a function of atomic number[13].

Figure 2-3 shows the dependence of the yield of backscattered and secondary electrons on the atomic number.

Detector types

Most modern microscopes are fitted with different detector systems for detecting either secondary or backscattered electrons. For detecting secondary electrons a scintillator-photomultiplier system is utilized. The secondary electrons strike the scintillator, which emits photons that the photomultiplier converts into pulses of electrons, which can be amplified and used for imaging.

Since the energy of the secondary electrons are too low to excite the scintillator they are accelerated by applying a bias voltage of approximately +10 keV. A collector at a positive potential of several hundred volts, surrounds the scintillator, and "collects" the low energy secondary electrons and thereby enables the SEM to "look around corners". The system is shown in Figure 2-4.

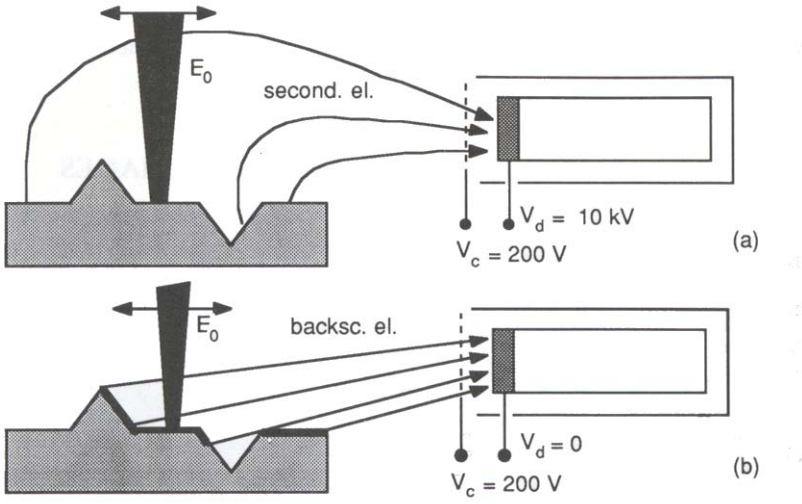

Figure 2-4 Path diagram of electrons reaching the detector (a) secondary electrons (b) backscattered electrons [14].

As can be seen from the figure there will also be a signal from the backscattered electrons, which follows a trajectory directly towards the detector, but the positive voltage applied to the collector is not high enough to "collect" the high energy backscattered electrons, which travel in other directions. By removing the bias, which accelerates the incoming secondary electrons, only the signal from the backscattered electrons hitting the scintillator is detected, however a modern SEM is usually fitted with a separate detector for detecting backscattered electrons.

Detectors for detecting backscattered electrons can either be of the scintillator-photomultiplier type or consist of solid-state detectors. The two different detector types are illustrated in Figure 2-5.

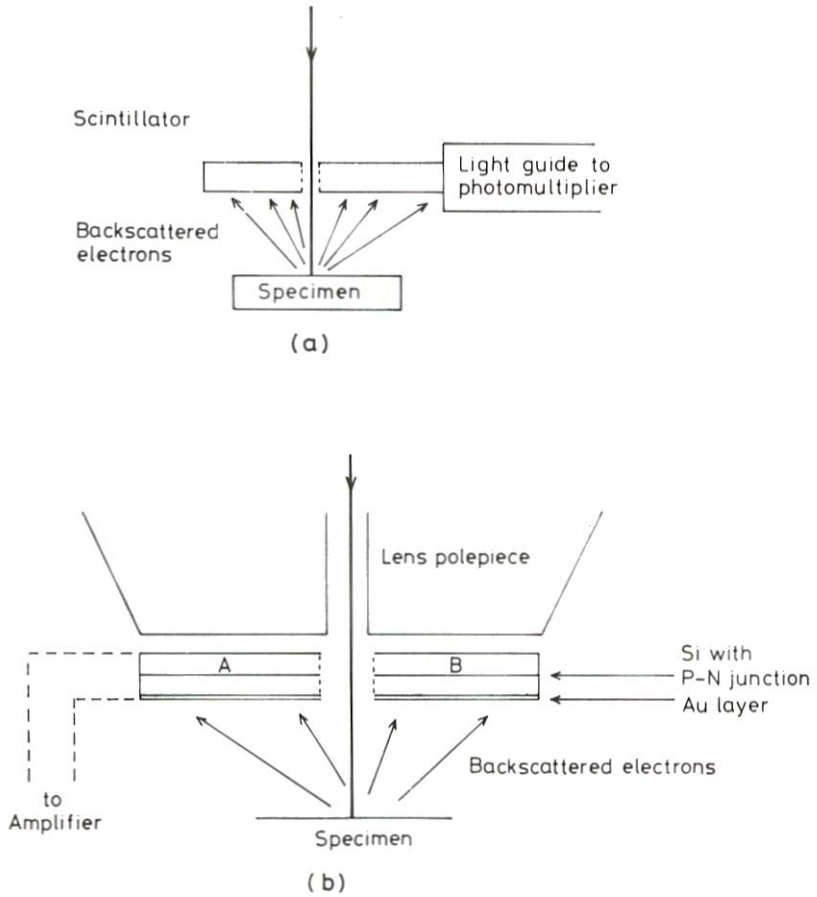

Figure 2-5 (a) Large area scintillator detector. (b) Solid state silicon detector with two elements A and B [14].

The detectors are designed to maximize the solid angle of collection, in order to gain the best possible signal to noise ratio. A multiple element backscatter detector makes it possible to enhance the topographic signals from a specimen. The two detectors A and B in Figure 2-5 will receive different topographic signals because they are located on different sides of the optical axis, therefore when the signals from A and B are subtracted from each other the signal from flat areas will to a first approximation be removed and topographic features will be enhanced. When the signals of the two detectors are added together the topographic features will be suppressed and the compositional contrast will be enhanced. An example of this is shown in Figure 2-6.

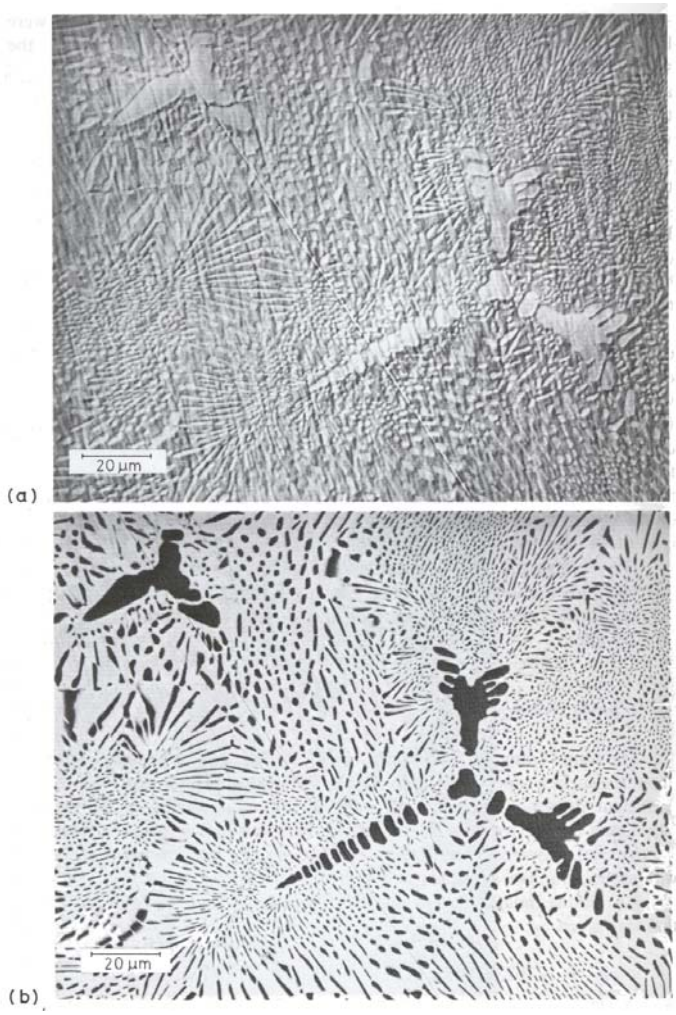

Figure 2-6 Backscattered images of a mechanically polished silver soldered joint (a) Topographic contrast arising from different resistance to abrasion of the phases, enhanced by subtracting the signals from the two elements of the detector. (b) Compositional contrast enhanced by adding the signals from the two detector elements [13].

X-rays

The bombardment of the specimen with the electron beam generates characteristic X-rays, which are used to obtain chemical information about the specimen. A modern SEM is usually fitted with EDS (Electron Dispersive X-ray Spectrometer) equipment for measuring the energy and the intensity of the X-rays emitted from a given test specimen.Figure 2-7 shows an example of a spectrum obtained by using EDS equipment.

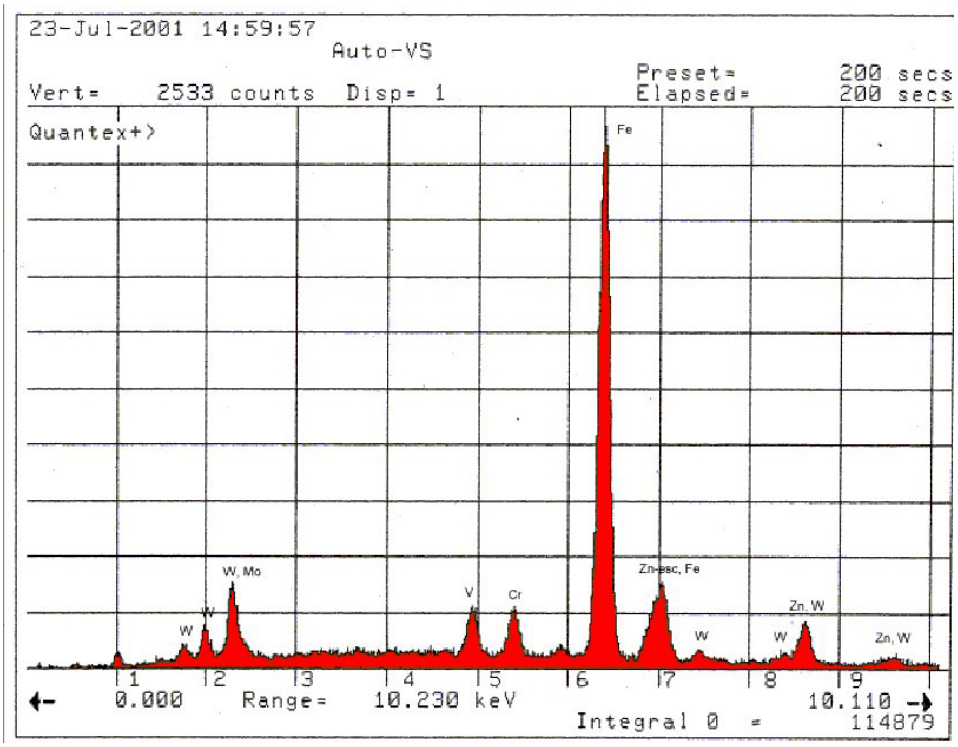

Figure 2-7 EDS spectrum from investigations on a high-speed steel.

The EDS equipment is controlled by a computer containing software, which has all the characteristic emission energies for all the elements stored, and therefore it is a simple matter to identify the elements giving rise to a peak in the spectrum.

The accuracy of EDS results is generally poor for analysis for elements lighter than sodium. Another limiting factor is that the energy resolution of the detector is poor, and therefore it is impossible to detect closely spaced lines such as for example Ag_L and Cd_L, which will result in only one peak in a spectrum. For these purposes it is necessary to use a dedicated microprobe facility equipped with a WDS (Wavelength dispersive spectrometer).

3 Experimental work

3.1 Test specimens

The tool samples, which have been used as a die for cold forging of a yoke, have an outer diameter of 63 mm. On Figure 3-1 one of the test samples is shown. The sample has been cut in half in order to reveal the place of failure.

As can be seen from the picture, the crack is located at an inner notch in the specimen, which is the location with the highest stress intensity (see Figure 3-2). The crack runs along the entire length of the tool sample, but the only place material has been removed is at the notch.

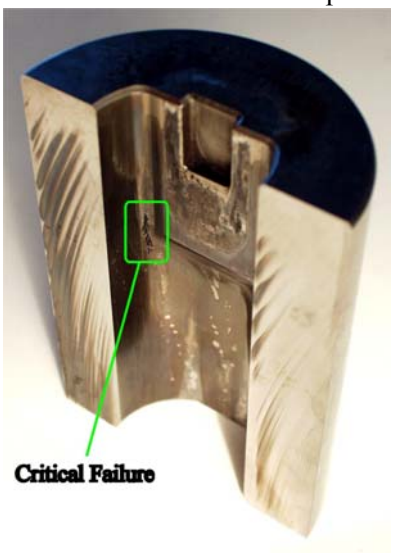

The specimen is symmetric and cracks are also initiated at the three positions similar to the one shown on the picture. Each tool specimen therefore contains 4 cracks.

Figure 3-1 Tool sample with visible crack.

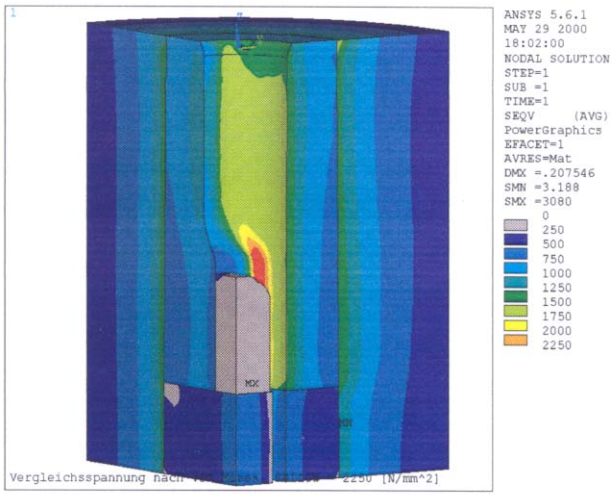

Figure 3-2 Von Mises stress distribution in the die [15].

Table 3-1 gives an overview of the test samples:

Table 3-1 Overview of test specimens.

	A	B	C
Material	Traditional P/M steel	Traditional P/M steel	Third generation P/M steel
Number of cycles to failure	62200	68800	~80000

The number of cycles for especially specimens A and B are a bit on the high side, since a large amount of specimens has failed at a much lower number of cycles. As a general observation the specimens made of "third generation" steel seem to last longer than the traditional steel.

The composition of the materials can be seen from Table 3-2.

Table 3-2 Composition of the tool steels (s790 in the Böhler P/M production line).

Chemical composition in wt.%				
C	**Cr**	**Mo**	**V**	**W**
1,28	4,2	5,0	3.1	6,4

The chemical composition of both the traditional steels and the "third generation" steel correspond to an AISI M3:2 standard and are delivered by Böhler.

3.2 Experimental procedures

Preparation of a plane polished surface (3 µm diamonds) has been performed for each of the three specimens followed by examination in both the LOM (Light Optical Microscope) and in the SEM (Scanning Electron Microscope).

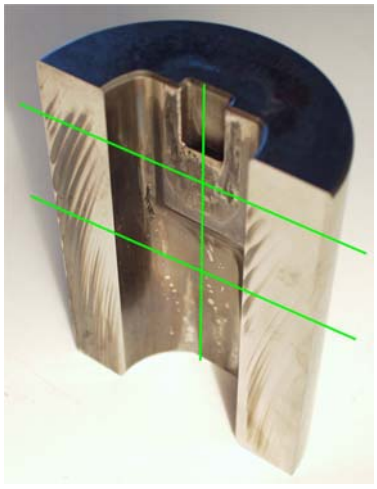

The crack formation in each tool sample was examined in the SEM, both before and after the specimens were ultrasonically cleaned in Alconox (see Appendix A). The specimens all had a hardness of approximately 62 HRC and were cut up at Struers A/S in Rødovre, Denmark, using an Exotom 100 and a Unitom 50. The cutting was done following the guidelines shown on Figure 3-3.

Figure 3-3 Tool sample with guidelines for cutting.

Afterwards the part of the specimen containing the crack was cut up from the back using a Struers Acutom 5. The specimen was cut almost all the way through, and then using a wedge in the saw cut and hitting it with a hammer opened the last part.

4 Results and discussion

4.1 Plane polished surfaces

The plane polished surfaces were examined in the LOM after treatment with Alconox and after etching with nital, and in the SEM using backscattered electrons in order to get a composition contrast. Figure 4-1 shows the LOM pictures after a treatment with Alconox.

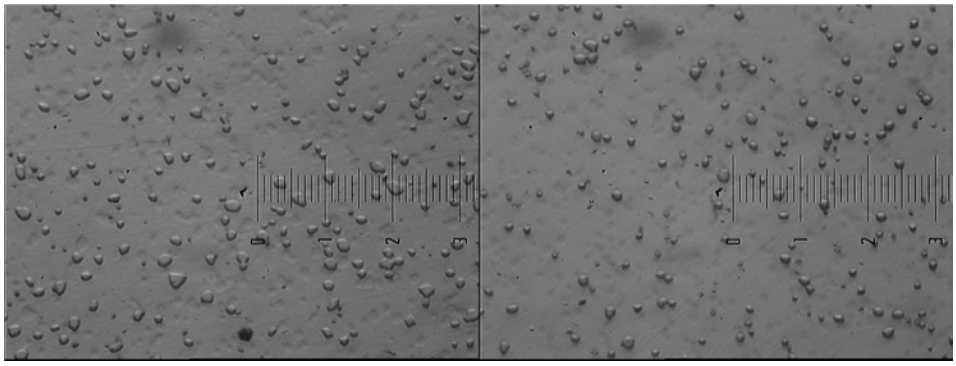

Figure 4-1 (a) and (b) LOM pictures of specimen A (to the left) and B (to the right) taken with 1010x magnification, one division on the scale equals 1 μm.

The fact that the carbides are so obviously exposed is because of the treatment in Alconox, and it is expected that the cleaning will have the same effect when used on the fracture surface in the crack. It can be seen that the carbides are finer in specimen C, as was expected.

The difference is a bit hard to see on the nital etched specimens in Figure 4-2. It could look as though there is a slightly larger tendency towards clustering of the carbides in specimen A. The difference in carbide distribution is easier to observe when viewing Figure 4-3.

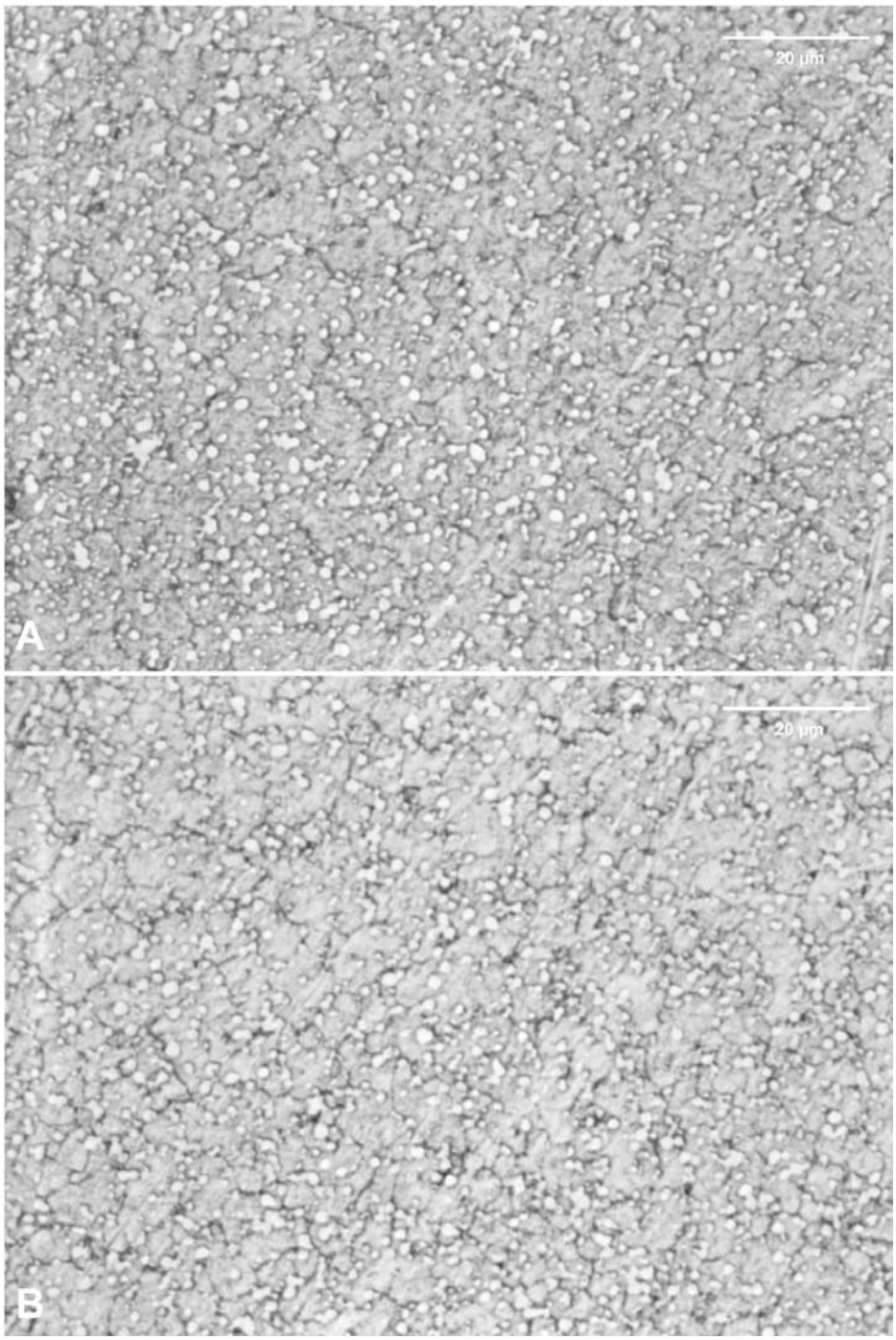

Figure 4-2 Nital etched specimens; (A) Specimen A. (B) Specimen C.

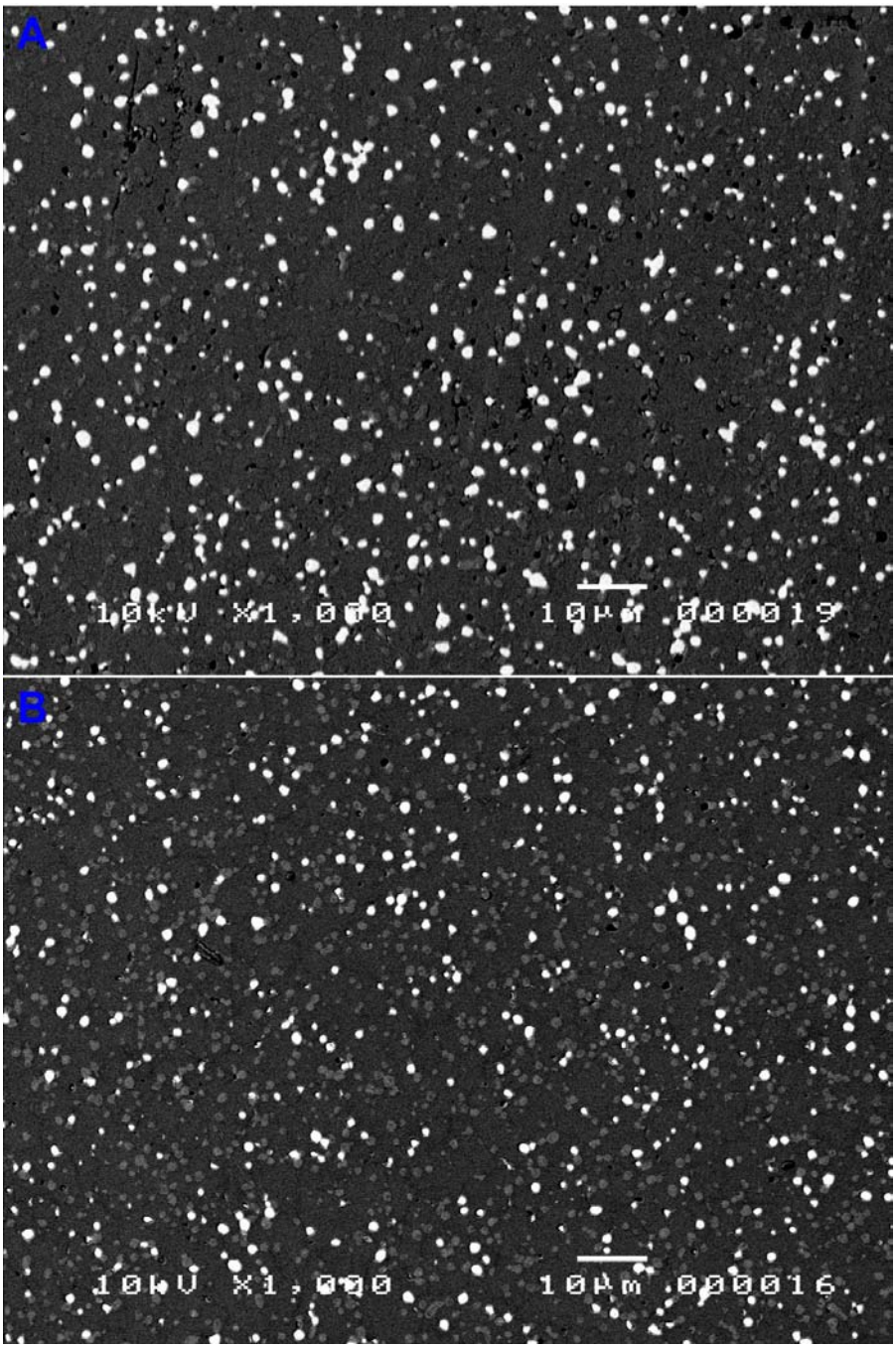

Figure 4-3 SEM-BE pictures of plane polished surfaces; (A) specimen A and (B) specimen C.

From Figure 4-3 it can be seen that there is quite a big difference in the carbon distribution for specimen A as compared to specimen C. The white carbides are M_6C carbides where M is either Mo or W. The reason that these carbides have the largest intensity is because of atom number contrast. The higher the atom number the higher the intensity of emitted backscattered electrons. The dark or grey carbides are MC carbides, where M is mostly V atoms. It can be seen that specimen A contains more and larger M_6C carbides than specimen C. Also there seems to be a tendency towards clustering of the M_6C carbides in specimen A. The difference in distribution of MC carbides is more difficult to ascertain, since the contrast difference between carbides and matrix is small especially in the picture of specimen A.

4.2 Fractures

Figure 4-4 shows the crack in specimen A before and after the cleaning treatment with Alconox. Figure 4-4 (a) shows that the crack is completely covered with small particles, which could possibly be residue from the lubricant (zinc-stearate) used in the tool during production and flakes from the matrix material. These particles make it very difficult to view the underlying fracture morphology.

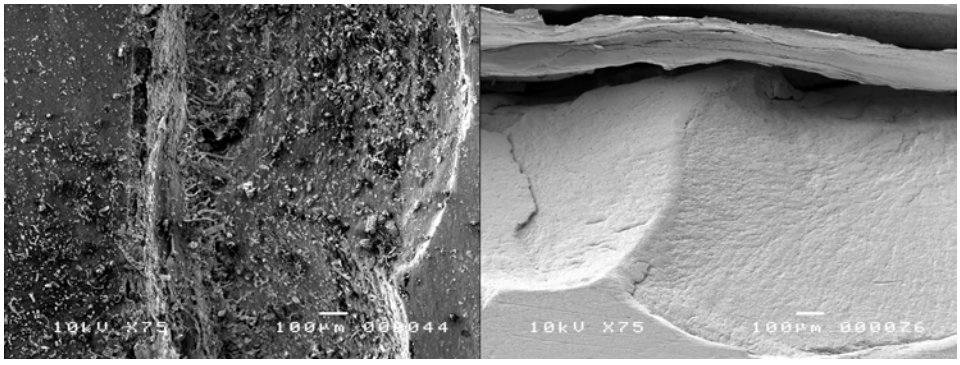

Figure 4-4 (a) and (b) SEM-SE pictures of the crack in specimen A. (a) Before cleaning with Alconox: The crack is covered with small particles of zinc-stearate. (b) After cleaning with Alconox.

That some of the particles are indeed zinc-stearate has been confirmed by the use of EDS (Energy Dispersive x-ray Spectroscopy), which gave a clear confirmation that zinc was present even though it is not part of the base-material (see Appendix B).

After the cleaning treatment all the particles have been removed and it is now possible to get a view of the actual fracture surface. However this is not without cost, since it seems that the treatment in Alconox is not entirely non-destructive (see appendix A for a discussion of this subject.)

Figure 4-5 shows low magnification SEM-SE pictures of the cracks in specimen A and B. The two cracks look very alike. It seems that the mechanism of crack growth/ expansion is chipping. When two or more small cracks grow together a flake of material is loosened and falls off whereby the crack is expanded.

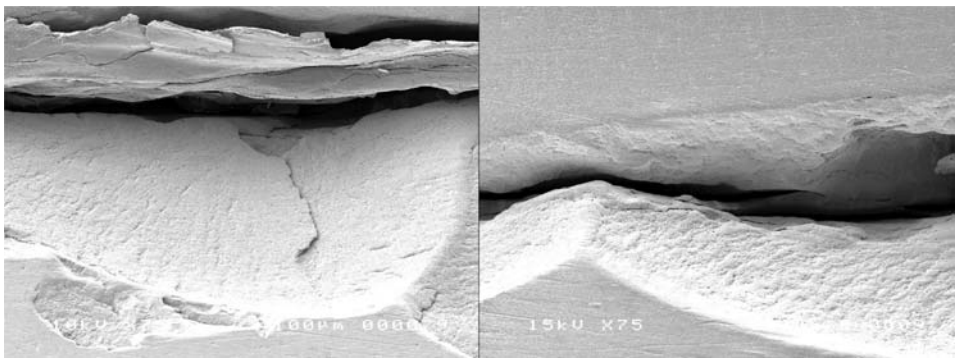

Figure 4-5 (a – to the left) and (b) SEM-SE pictures of the cracks. (a) Crack in tool sample A (b) Crack in tool sample B.

Figure 4-6 (a,b,c,d) shows the end of the crack in tool sample A at higher magnifications, and it reveals a highly porous microstructure, which is certainly not what is expected from a tool steel. The pictures show several secondary cracks, which seem to have grown from the primary crack. On the surface the carbides have been laid bare, and in several places they have dislodged. This might however be an effect of the prior treatment in Alconox.

It must also be considered that specimen A and B has run quite a large amount of cycles (~60000) compared to the average tool made of traditional AISI M3:2 steel (5000-20000) before being taken out of production. Therefore one might expect that the effects that lead to failure may show in an especially grave manner in these specimens due to their extended lifetime. The crack in tool sample B is similar of appearance to the one seen in tool sample A.

Figure 4-6 (e,f,g,h) shows the crack in specimen C at similar magnifications. It is a general observation, that the surface of the C-specimen does not look as worn as the other specimens, even though it looks as though the mechanism of crack growth is the same. This corresponds well with the fact that the specimens produced from “third generation” steel generally have a longer lifetime.

Another interesting observation made from these pictures is that the inner surface of the tool sample seems to be covered with long abrasive marks mostly oriented in the direction of the mass flow in the tool. These marks probably originate from the actual use of the tool during production and they are present even far from the crack. The abrasive marks are clearly more distinct on specimen A and B than on specimen C.

The abrasive marks on specimen B that can be seen on Figure 4-6 (a) and (b) are also present in areas far from the primary crack but still near the notch. This can be seen on Figure 4-7. If looked closely upon, the two pictures show quite a few micro cracks and several cracked carbides. It might be possible, that the abrasive marks have had an influence on the initiation of the fatigue crack at the place in the tool, where the highest stress-concentrations are found.

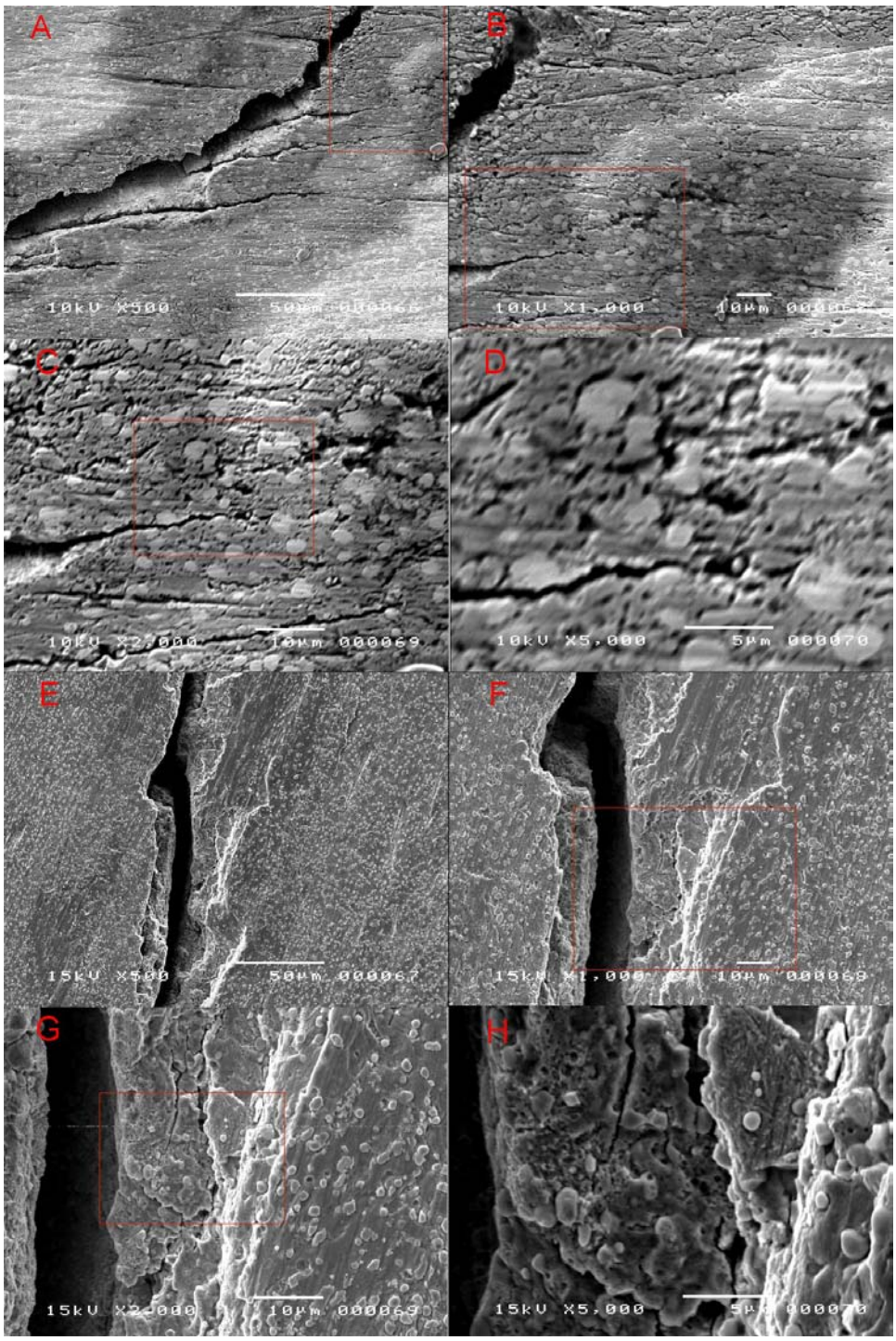

Figure 4-6 SEM-SE pictures; (a,b,c,d) show the crack in specimen A at different magnifications, and (e,f,g,h) show the crack in specimen C.

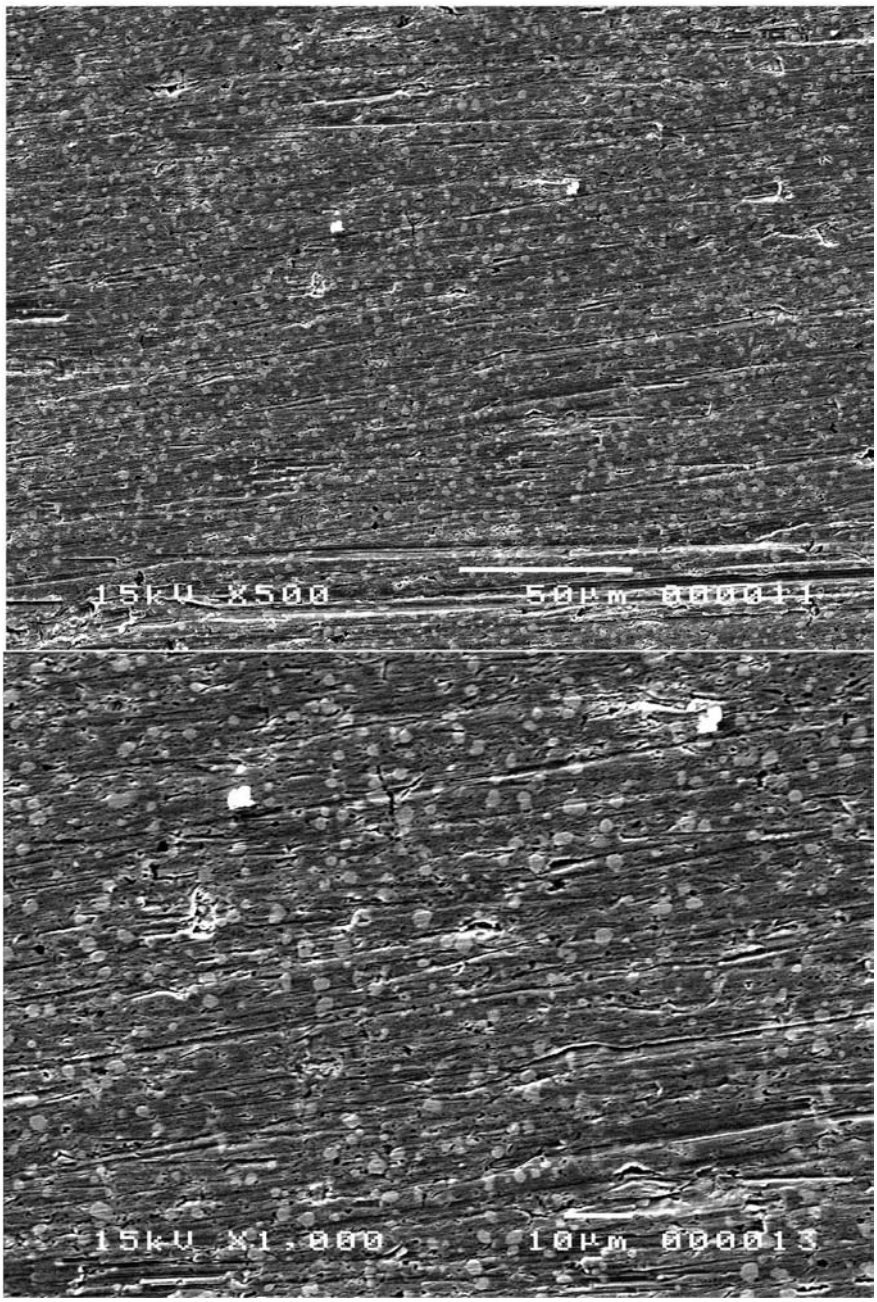

Figure 4-7 SEM-SE pictures of tool sample B at an area far from the crack but still in the vicinity of the notch.

4.3 Opened specimen

"Opening" of the cracked specimens reveals that the complex nature of the stress-situation around the notch in the tool due to the prestressing makes the direction of crack-growth equally complex and difficult to predict. This made it very hard to open up a crack without at the same time destroying it. The only crack successfully opened was from specimen C, but it must be expected that the overall mechanism of crack growth in this specimen is the same as for the other two specimens, so even though there might be microstructural differences the overall features should be comparable.

Below the part of the crack that is observable on the surface, the crack runs deep into the specimen as can be seen on Figure 4-8. The crack has occurred in a brittle cleavage like manner near the surface, but some distance from the surface the appearance of the crack changes abruptly.

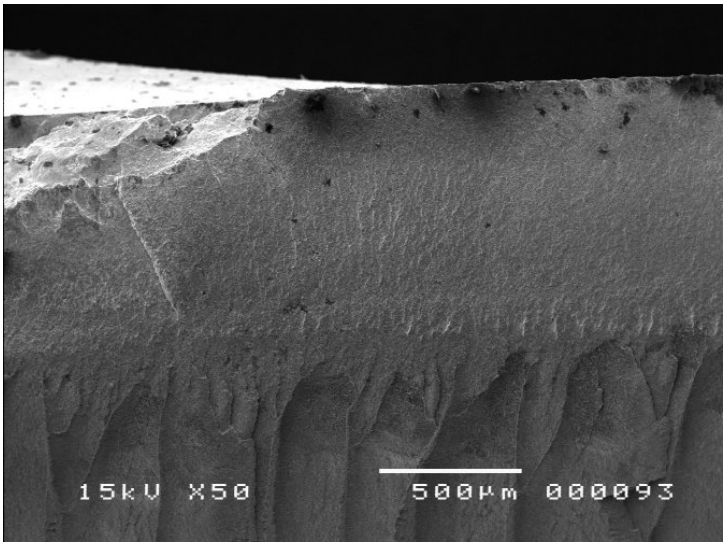

Figure 4-8 SEM-SE picture of the opened crack in specimen C. In the top left corner, the part of the crack that is visible in the unopened specimen can be seen. In the lower part of the picture the crack running inside of the specimen can be observed.

Several ridges can be observed where the crack front has been arrested (See lower part of Figure 4-8). The markings are much too coarse to be striations, which are seen, in more ductile materials where crack tip blunting occurs. It is likely that these ridges originates from the procedure used for opening up the specimen. The specimen was cut up from the back opposite the visible fracture with a rotating saw while the specimen was oscillated ±20° in order to avoid the saw getting stuck. The ridges are probably the result of fatigue crack growth due to the repeated impacts between saw and specimen. If it had been possible to cut up the specimen without having to oscillate it these markings would probably not have been observed.

Cracking of carbides

As discussed in the theory part cracked carbides can be the initiation point of micro cracks. In specimen C several cracked carbides can be observed in the area near the bottom of the crack as can be seen from Figure 4-9. Specimen A

and B contain a volume fraction of cracked carbides of the same magnitude as specimen C.

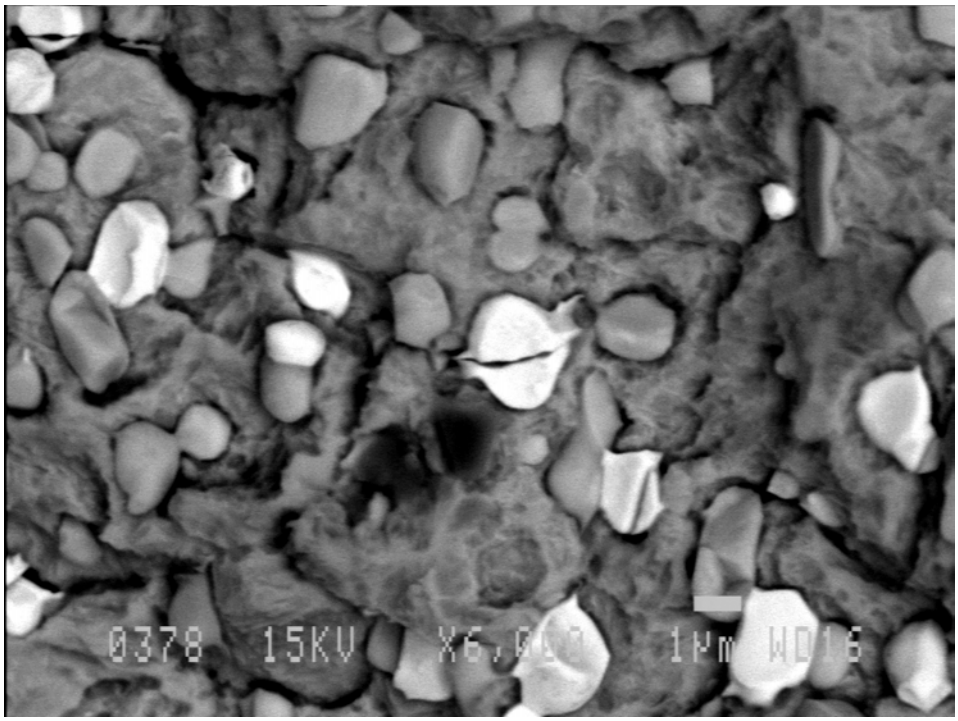

Figure 4-9 SEM-BE picture of cracked carbides in specimen C.

It is not possible to link the initiation of the main crack in the tool specimens directly to the cracking of carbides in the area where the fracture takes place. It is obvious that the dies have been used for several production cycles after the initiation of the crack has taken place. The die is taken out of production when the fracture damage is so grave that the final product does not make it through the quality control. In order to establish the exact reason for the crack initiation it would be necessary to analyse a die specimen where the crack has only just initiated.

5 Conclusion

When comparing the plane polished surfaces of the specimens constructed in traditional P/M high-speed steel with the one constructed in third generation P/M steel the overall impression is that the third generation steel contains finer carbides, and that there is a slightly larger tendency towards clustering of the carbides in the traditional steels.

The macroscopic look of the fracture in the traditional and the third generation steels looks very alike.

The inner surface of the dies constructed in the traditional steel looks much more worn than the die constructed in third generation steel even though the last mentioned has run the most production cycles. This implies that the third generation steel has a higher resistance against abrasive wear. The observed abrasive marks could very likely play a role in the initiation of the fatigue cracks.

It is not possible to link the failure with cracking of carbides at the critical position in the cold forging dies since the initial point of failure can no longer be observed due to chipping off of material.

5.1 Future work

It would be nice to be able to quantify the difference in microstructure. QIA (Quantitative Image Analysis) on either X-ray maps or backscattered electron images of the plane polished specimens would therefore be very interesting.

There could also very likely be differences in other areas than just size and distribution of carbides. For example in the characteristics of the matrix and in the size of grains.

6 Appendix A: Alconox

The purpose of this appendix is to evaluate the use of Alconox for the cleaning of fracture surfaces on an AISI M3:2 P/M steel.

The use of Alconox is favourable since it is biodegradable and non poisonous, which makes it much easier to handle than for example acid or organic solvents. However it has been observed that Alconox induces certain changes in the morphology of the surface of test-specimens, which become more pronounced with increased process time.

Since it is critical that the fracture surfaces do not undergo any treatments that drastically change the morphology and thereby perhaps obscure the mechanism that was the reason behind the fracture, it is necessary to know the effect of all used treatments in detail.

Therefore this appendix aims to clarify both the general effect of a cleaning treatment using Alconox and the effect of process time

Description of Alconox taken from www.alconox.com

Concentrated, anionic detergent for manual and ultrasonic cleaning. Free rinsing to give you reliable results without interfering residues.

Ideal for cleaning contaminants from glassware, metals, plastic, ceramic, porcelain, rubber and fibreglass.

Excellent replacement for corrosive acids and hazardous solvents. USDA authorized. Dilute 1:100. pH 9.5.

Figure 6-1 Alconox.

6.2 Background/ Theory

The treatment in Alconox is described in ASTM STP 827, 1984, p. 267 and also in the "Metals Handbook, Ninth Edition, Volume 12, Fractography", page 75:

The cleaning solution is prepared by dissolving 15 g of Alconox powder in a beaker containing 350 mL of water. The beaker is placed in an ultrasonic cleaner preheated to about 95 °C (205 °F). The fracture is then immersed in the solution for about 30 min. rinsed in water then alcohol, and air dried.

Figure 6-2 shows an example of the use of ultrasonic cleaning with Alconox on a fracture surface.

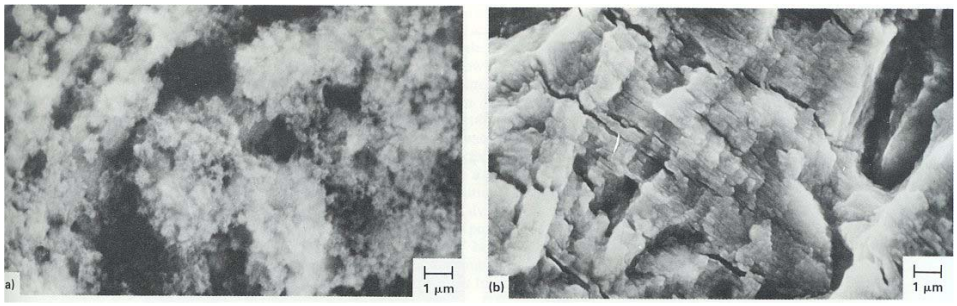

Figure 6-2 (a) and (b) Fatigue precrack region (a) Before cleaning in Alconox. (b) After cleaning in Alconox [11].

Prolonged exposure in the Alconox solution causes a chemical etching of the test specimen and can cause the dislodging of originally embedded inclusions (See Figure 6-3 (a) and (b)).

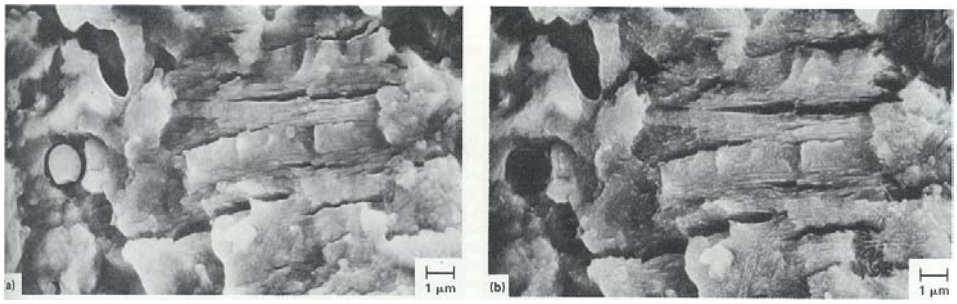

Figure 6-3 (a) and (b) Effect of increasing the ultrasonic cleaning time in a heated Alconox solution (a) 30 min. (b) 3.5 h. Note the dislodging of the inclusion and the chemical etching of the fracture surface [11].

According to the Metals Handbook the prolonged treatment (more than 30 minutes) has very little cleaning effect and should therefore be avoided.

6.3 Experimental work

Experiments have been performed on test specimens of AISI M3:2 steel with a composition that can be seen from Table 6-1.

Table 6-1 Composition of the AISI M3:2 steel.

Composition range	Chemical composition in %							
	C	**Cr**	**Mo**	**V**	**W**	**Co**	**Mn**	**Si**
Min	1,17	3,80	4,70	2,70	6,00	-	0,00	0,00
Max	1,27	4,20	5,20	3,20	6,70	-	0,40	0,45

The test specimens are cleaned ultrasonically at 50-60°C in a solution prepared from 15g Alconox and 350mL water. The reason that a lower temperature is used, instead of the 95°C described in the standard, is due to a limit imposed by

the available ultrasonic bath (Branson 2200) which can't operate at higher temperatures. This however shouldn't have any significant influence on the result.

A polished surface has been prepared and examined before and after the treatment with Alconox in a LOM (Light-Optical Microscope)

Three rectangular specimens with approximate dimensions 1,0-2,5-0,3cm were weighed before and after the treatment in Alconox, making it possible to observe if a significant amount of material disappears during the treatment.

Furthermore the fracture surface of a ”fatigue” crack located at an inner notch in a tool used for cold working has been examined in the SEM (Scanning Electron Microscope) before and after the treatment in Alconox.

6.4 Results and discussion

Plane polished surface

As can be seen from Figure 6-4 there is a distinct difference in the surface morphology of the specimen before and after the treatment with Alconox. Apparently Alconox etches some of the matrix material while leaving the carbides virtually untouched.

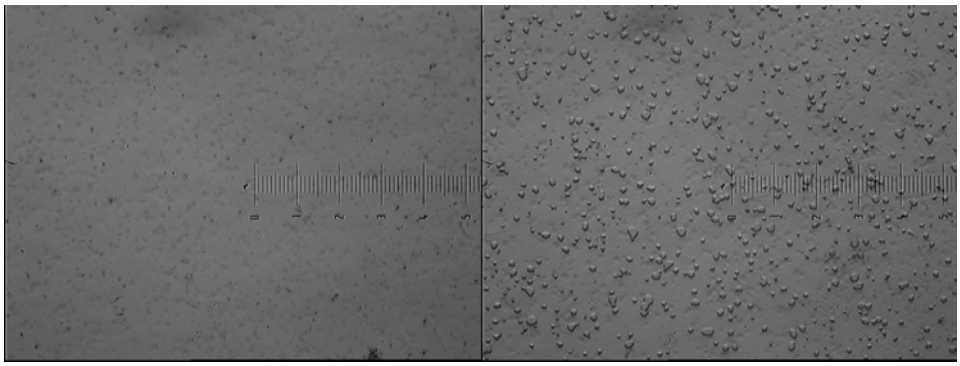

Figure 6-4 (a) and (b) LOM-pictures taken with 646x magnification. One division on the scale equals 1 μm. (a) Before treatment with Alconox. (b) After ½ an hour treatment with Alconox.

The specimen in Figure 6-4 (a) was ultrasonically cleaned for 10 min. in acetone before being examined in the LOM, and therefore it seems unlikely that the material removed during the treatment with Alconox could be just grease or paste residue from the polishing.

Also the amount of material removed seems to be too much to indicate the removal of an oxide-layer. An oxide layer would also reform itself after a given amount of time, which would mean that the surface after treatment with Alconox would after some time return to it’s original state. This is not observed.

The treatment with Alconox gives a rather nice indication of the distribution of carbides in the steel. But during the investigation of a fracture surface this effect will not be favourable since it changes the morphology of the surface, thereby making it difficult to assess whether an effect originates from the fracture mechanism or from the treatment during cleaning.

Varying the treatment time

In order to estimate the effect of the treatment time, the polished specimen was examined in the LOM after 0, 10, 15, 20, 30, 60 and 90 minutes. Only one specimen was used for this examination. This means that the specimen was taken out of the hot ultrasonic bath at the given time-intervals, and then reinserted after examination. The result can be seen on Figure 6-5.

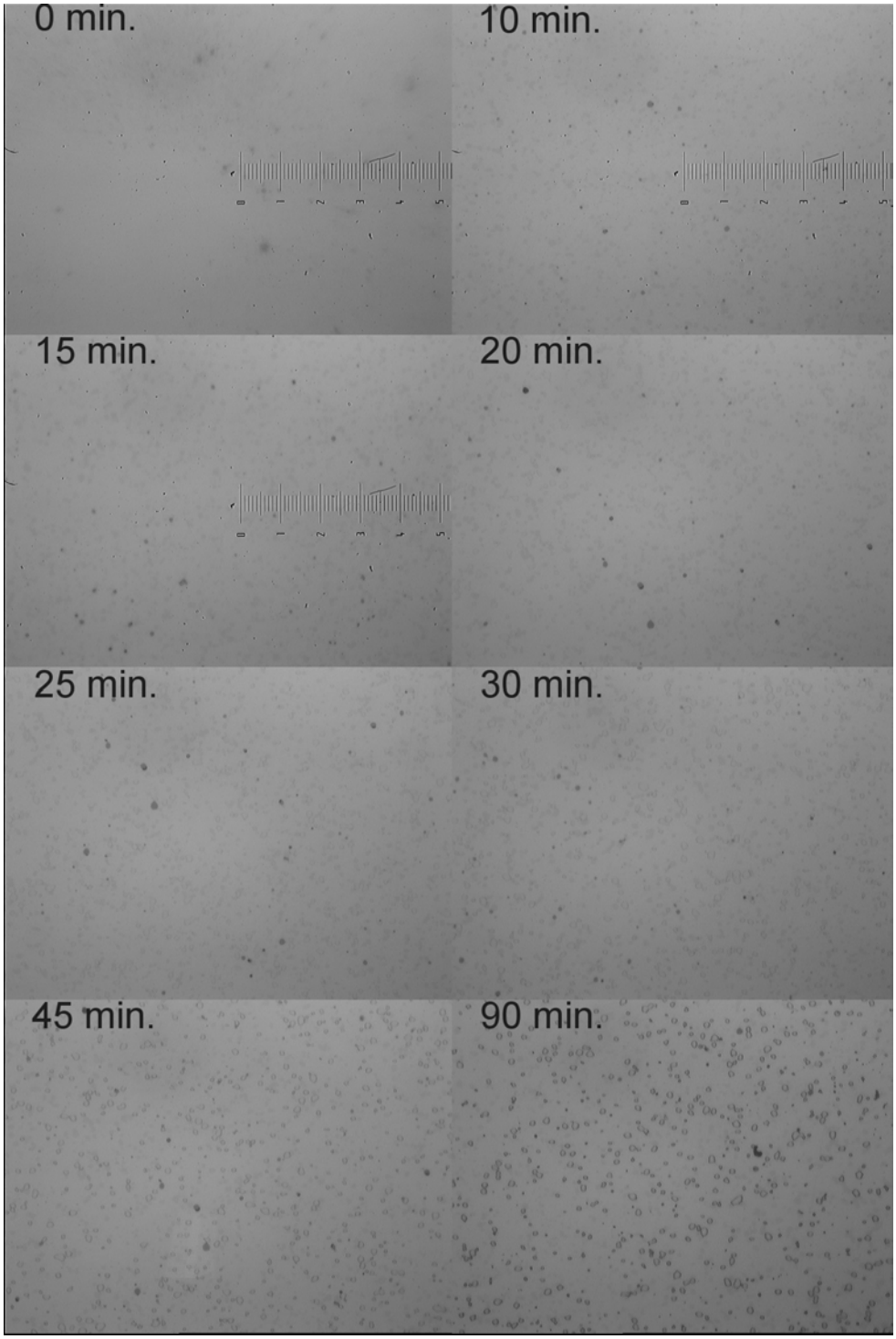

Figure 6-5 LOM-pictures of the plane polished surface after treatment in Alconox in 0, 10, 15, 20, 25, 30, 45 and 90 minutes. taken with 646x magnification. One division on the scale equals 1 μm.

It looks as though the specimen is not attacked as heavily when it is taken out of the ultrasonic bath at regular intervals for examination (compare Figure 6-4 and Figure 6-5). This might be explained by the formation of a protective oxide-layer each time the specimen is taken out of the hot Alconox solution. At the given pH-values (7 and 9,5) Fe is in the passive area.

Assuming that Alconox removes the oxide layer it might be expected that allowing the oxide layer to reform during the cleaning treatment (removing the specimen from the Alconox-solution) delays the overall dissolution of the matrix-material. It would therefore be more correct to use one test-specimen for each test-time.

Weight loss

Before the Alconox treatment the three specimens A, B and C were cleaned ultrasonically in acetone for 15 minutes.

The specimens were weighed using a Messler AE 163 precision weight.

The dimensions of the test specimens were:

A: 2,025cm-1,020cm-0,305cm, Volume = 0,630cm^3, Area = 5,988cm^2
B: 2,025cm-1,020cm-0,295cm, Volume = 0,609cm^3, Area = 5,928cm^2
C: 2,025cm-1,020cm-0,190cm, Volume = 0,392cm^3, Area = 5,288cm^2

The measured weights and weight losses can be viewed in Table 6-2 and Table 6-3.

Table 6-2 Weight and weight loss of specimens treated in Alconox.

	A/ g	**A-loss**/ g	**B**/ g	**B-loss**/ g	**C**/ g	**C-loss**/ g
0 min.	5,02237	-	4,90106	-	3,21905	-
30 min.	5,02154	0,00083	4,90036	0,00070	3,21838	0,00067
60 min.	5,02093	0,00144	4,89968	0,00138	3,21790	0,00115
150 min.	5,01847	0,00390	4,89723	0,00383	3,21586	0,00319

Table 6-3 Weight loss per time and surface area.

	A/ $\frac{\mu g}{min \cdot cm^2}$	**A/** $\frac{\mu g}{min \cdot cm^2}$	**A/** $\frac{\mu g}{min \cdot cm^2}$
30 min.	4,620	3,936	4,223
60 min.	4,008	3,880	3,624
150 min.	4,342	4,308	4,022

The weight loss per minute per surface area measured in cm^2 is approximately equal to 4 $\frac{\mu g}{min \cdot cm^2}$ for all the measurements (See Table 6-3).

This weight loss is, as could be expected from the pictures of the plane polished surfaces, very small and gives no cause for concern.

Fracture of a tool

The Alconox treatment was used to clean a crack located at an inner notch in a tool die used for cold forging. On Figure 6-6 one half of the fractured tool is shown. The cleaning was necessary since prior to the cleaning procedure the crack was covered with residue of zinc-stearate (see Appendix B) that was used as a lubricant in the original tool.

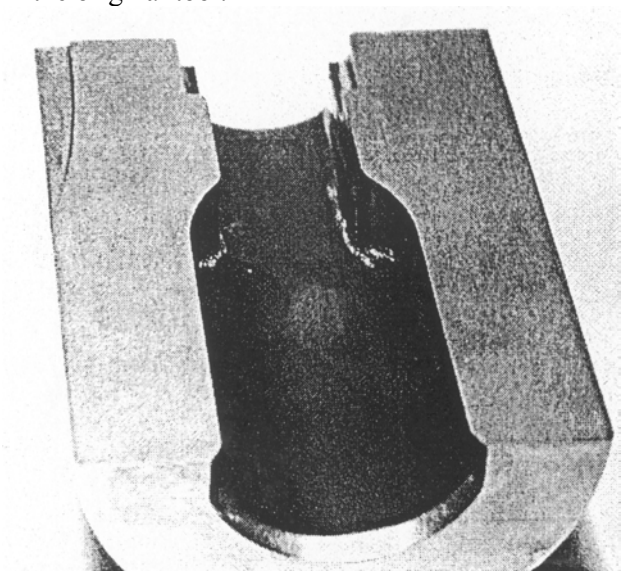

Figure 6-6 The die, cut in half to show two of the four cracks initiated at the inner notch.

On Figure 6-7 enlarged views of the crack before and after the treatment in Alconox are shown.

The zinc-stearate-particles almost completely obscure the underlying fracture morphology and it is necessary to remove them in order to get a closer look at the actual surface. By comparing Figure 6-7 (a) and Figure 6-7 (b) it can be seen that the treatment in Alconox effectively removes the disturbing particles thereby revealing the fracture surface.

By prolonging the treatment however it is revealed that the Alconox treatment not only affects the disturbing particles, it is also capable of removing parts of the base material. This can be seen by comparing picture Figure 6-7 (b) and Figure 6-7 (c). On figure (b) a large “flake” is visible in the top of the picture, but after 90 minutes of treatment the flake is no longer present and can’t be seen in picture (c). It has been loosened by the prolonged treatment in Alconox. It is most likely the combined effect of the chemical etching by Alconox and the mechanical agitation from the ultrasonic bath that has caused this.

Taking a closer look at the microstructure in Figure 6-8 it seems as though the carbides are laid bare and at several places they have dislodged. Looking back at the effect that the Alconox treatment had on the plane polished surfaces, this could very well be because of the cleaning procedure.

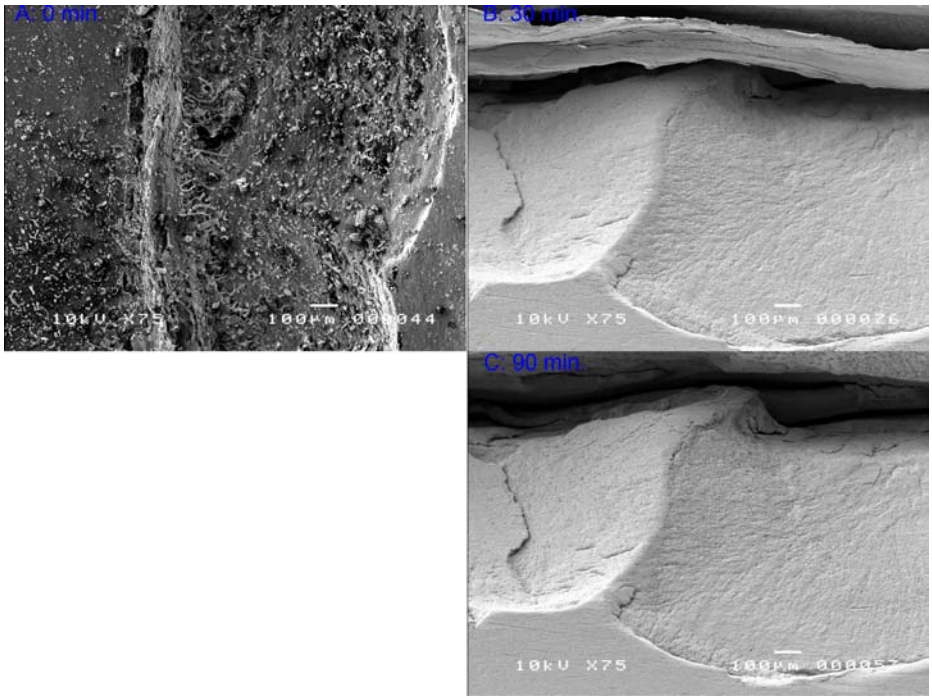

Figure 6-7 (a), (b) and (c) SEM-SE pictures of a crack located at a notch inside a tool die used for cold forging. (a) Before treatment with Alconox: The crack is covered with small particles of zinc-stearate and oxides. (b) After ½ hour of treatment with Alconox: Same location in the crack as in (a) turned 90°. (c) Same as (b) but after 1½ hour of treatment in Alconox. Notice that a large part present in the top of picture (b) is no longer present in picture (c).

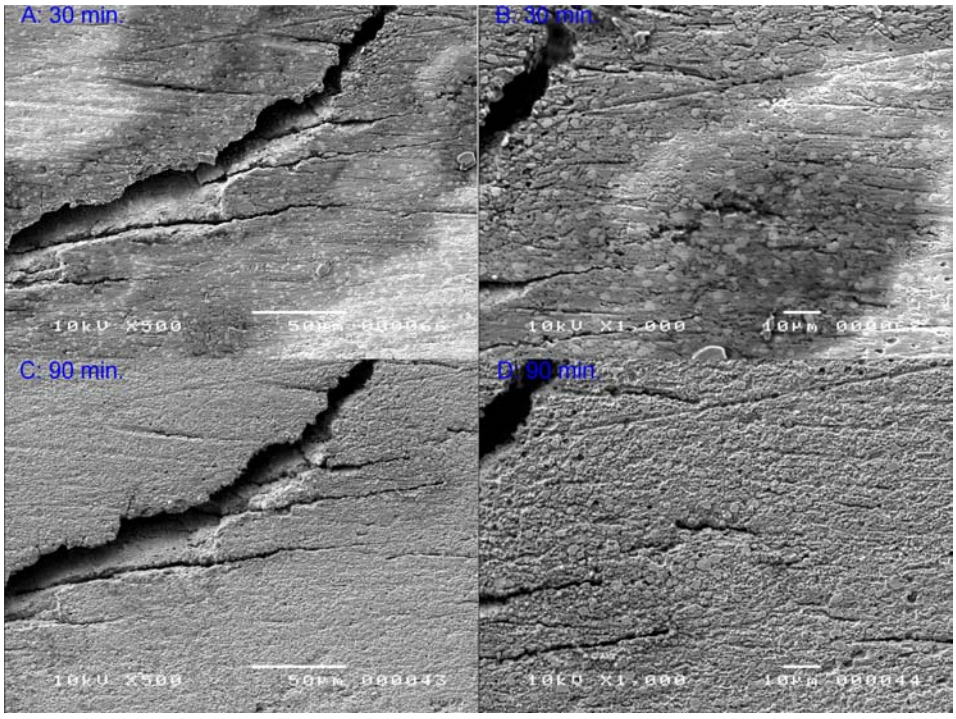

Figure 6-8 (a), (b), (c) and (d) (a) Shows the highly porous area surrounding the crack after ½ hour of treatment in Alconox. (b) Shows the top right area of picture (a) also after ½ hour. On both pictures the carbides are highly exposed! (c) and (d) show the same area as (a) and (b) respectively but after 1½ hour of treatment in Alconox.

On Figure 6-8 (a) and (b) it can be seen that the material around the crack is extremely porous and at several places it looks as though the carbides have fallen out of the material. It might be expected that this is the result of the cleaning procedure.

On Figure 6-8 (c) and (d) it is even clearer that the matrix material has been etched, since most of the crack-edges seem to have been smoothened or rounded off. In picture (d) it is possible to view the bottom of most of the small cracks, which was not possible in picture (c), indicating that surface material has been removed whereby the cracks have been made shallower.

The change in microstructure is quite significant from (a) to (c) and from (b) to (d). Therefore it is obvious that the treatment in Alconox does indeed change the morphology of the fracture surface especially at prolonged treatment times.

One specimen was cleaned for only 15 minutes, but still had disturbing oxides present near the crack, which indicates, that a longer process time is necessary.

6.5 Conclusion

Alconox is a very useful product for the cleaning of fracture surfaces on tool steels, as long as one keeps the observed side effects in mind.

The strength of Alconox is that it is extremely easy to handle and no more toxic than a normal detergent that can be bought in an ordinary supermarket. It removes all the disturbing oxides and residue from the lubricating oil.

The cost is a change in the surface morphology. Part of the ferrite-matrix is etched and thereby the carbides are laid bare. The weight loss observed during the cleaning is negligible, but the visible effect is significant and should always be kept in mind when viewing surfaces cleaned in Alconox. In order to minimise the unwanted change in morphology extended treatment (above approximately 30 minutes) should be avoided.

If the purpose of the cleaning is to observe the distribution and the behaviour of the carbides in the tool steel (for example when looking for fractured carbides as possible crack initiation sites) the treatment in Alconox is excellent since it both cleans the specimen and enhances the effect looked for.

7 Appendix B: EDS-Analysis

The purpose of the examination is to find out whether zinc is present in the particles covering the fracture surface, thereby proving that the particles consist of zinc-stearate, which was used as lubricant in the examined tool sample.

Figure 7-1 shows an overview of the area examined during the analysis. Four different analyses were performed. One overall scan of the entire area marked by a large rectangle (Krda1). Two spot analyses centred at particles marked by circles (Krda2 and Krda4), and one spot analysis centred at an area without particles marked by a triangle (Krda3).

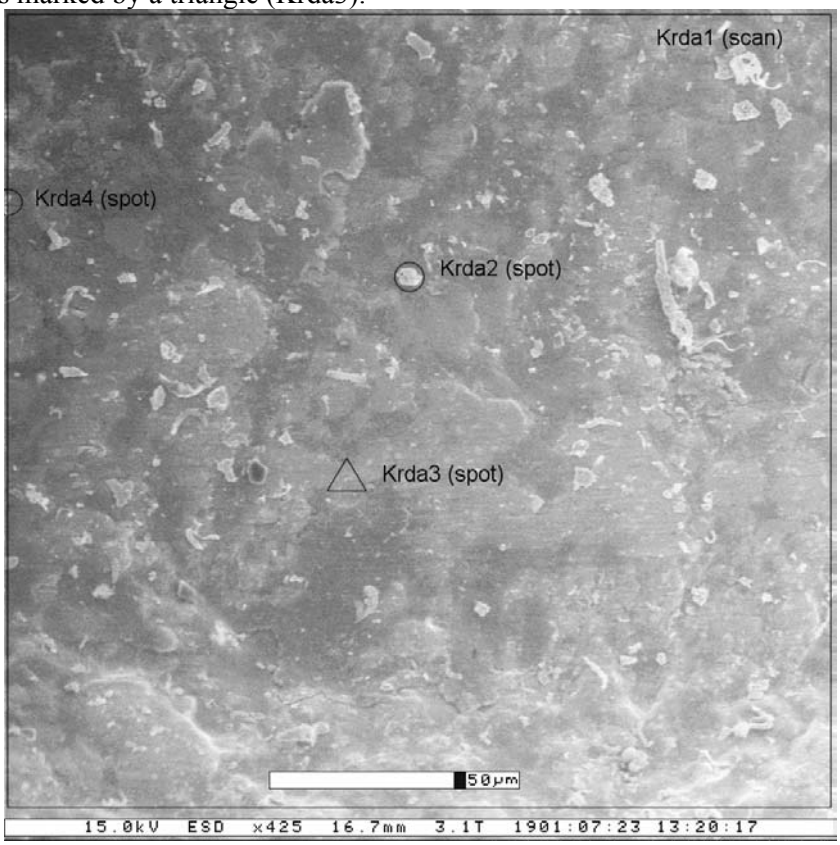

Figure 7-1 Overview of the scan-area examined during the EDS-analysis. Krda1: Scan of the total area. Krda2 and Krda4: Spot scans of particles. Krda3: Spot scan of area free of particles.

The expected result would be that, Krda1 showed some signs of the presence of zinc, while Krda2 and Krda4 would show a higher content, and Krda3 a lower content of zinc.

As can be seen from the following pages the results agree nicely with this assumption, and it is safe to conclude, that the surface particles contain zinc. Since the base-material does not contain any zinc it seems highly likely that the particles consist of zinc-stearate-residue from the lubricant used in the tool during production.

KBDA01

23-Jul-1901 14:56:52 AHANX

Accelerating voltage	20.0 KeV
Beam - sample incidence angle	90.0 degrees
Xray emergence angle	17.1 degrees
Xray - window incidence angle	0.1 degrees

STANDARDLESS EDS ANALYSIS
(XPP QUANTITATION)

ELEMENT & LINE	WEIGHT PERCENT	ATOMIC PERCENT*	PRECISION 2 SIGMA	COMPUTED K-RATIO**
V KA	3.55	4.40	0.13	0.0337
Cr KA	3.36	4.08	0.12	0.0348
Fe KA	62.55	70.76	0.63	0.6121
Zn KA	11.26	10.88	0.40	0.0988
Mo LA	10.35	6.82	0.36	0.0616
W LA	8.93	3.07	0.65	0.0666
TOTAL	100.00			

ITERATIONS 6

*NOTE: ATOMIC PERCENT is normalized to 100

**NOTE: K-RATIO = K-RATIO x R
where R = reference(standard)/reference(sample)

NORMALIZATION FACTOR: 1.000

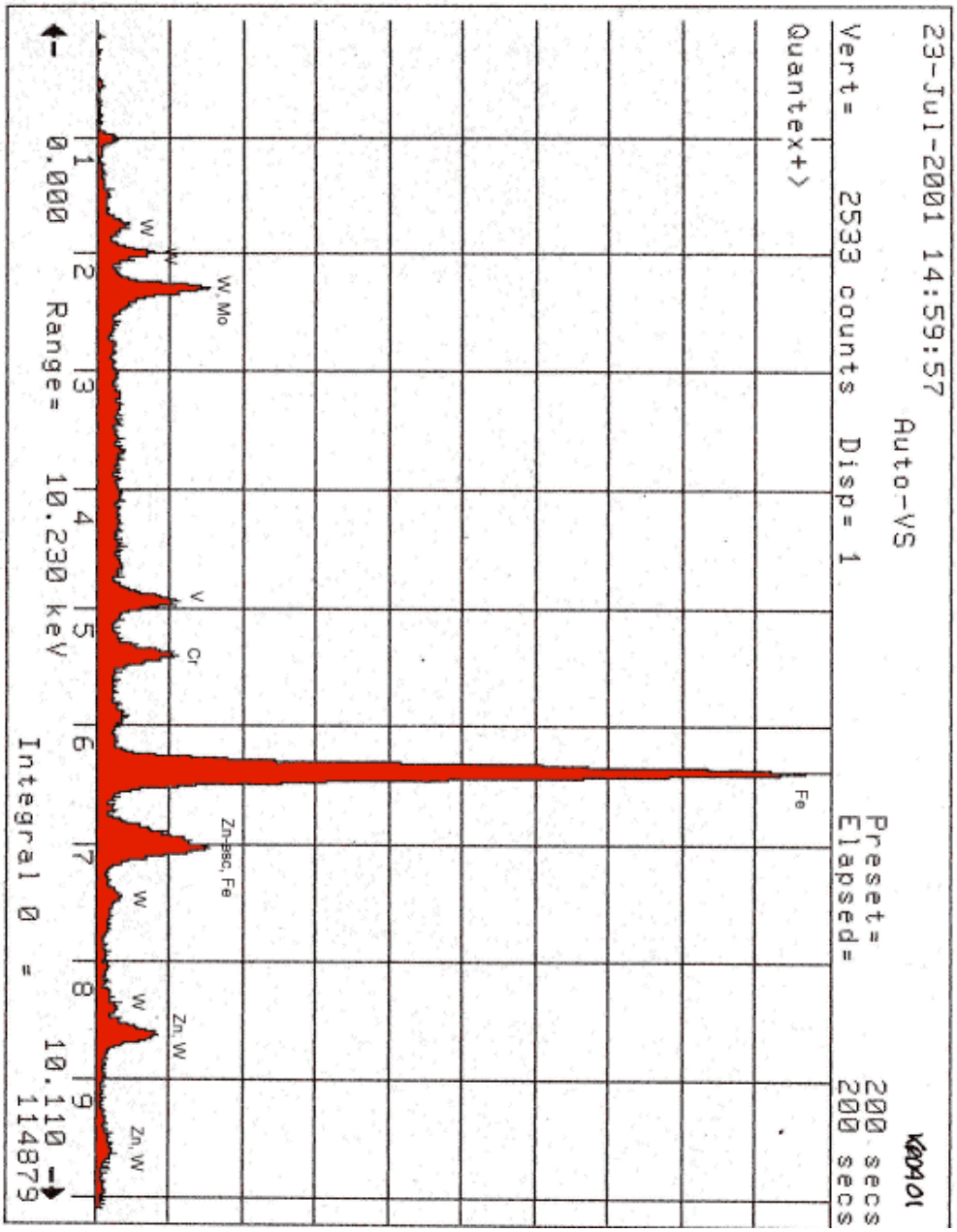
23-Jul-2001 14:59:57
Auto-VS
Vert= 2533 counts Disp= 1
Quantex+>
Preset= 200 secs
Elapsed= 200 secs
Fe
W
W, Mo
V
Cr
Zn-esc, Fe
W
Zn, W
W
Zn, W
0.000
Range= 10.230 keV
Integral 0 = 10.110
114879

KRDA02

23-Jul-1901 15:22:54 krda02

Accelerating voltage 20.0 KeV

Beam - sample incidence angle 90.0 degrees

Xray emergence angle 17.1 degrees

Xray - window incidence angle 0.1 degrees

STANDARDLESS EDS ANALYSIS
(XPP QUANTITATION)

ELEMENT & LINE	WEIGHT PERCENT	ATOMIC PERCENT*	PRECISION 2 SIGMA	COMPUTED K-RATIO**
V KA	2.45	3.01	0.11	0.0235
Cr KA	2.72	3.27	0.12	0.0285
Fe KA	64.06	71.90	0.68	0.6331
Zn KA	14.39	13.80	0.48	0.1261
Mo LA	7.75	5.06	0.33	0.0451
W LA	8.64	2.95	0.69	0.0643
TOTAL	100.00			

ITERATIONS 6

*NOTE: ATOMIC PERCENT is normalized to 100

**NOTE: K-RATIO = K-RATIO x R
where R = reference(standard)/reference(sample)

NORMALIZATION FACTOR: 1.000

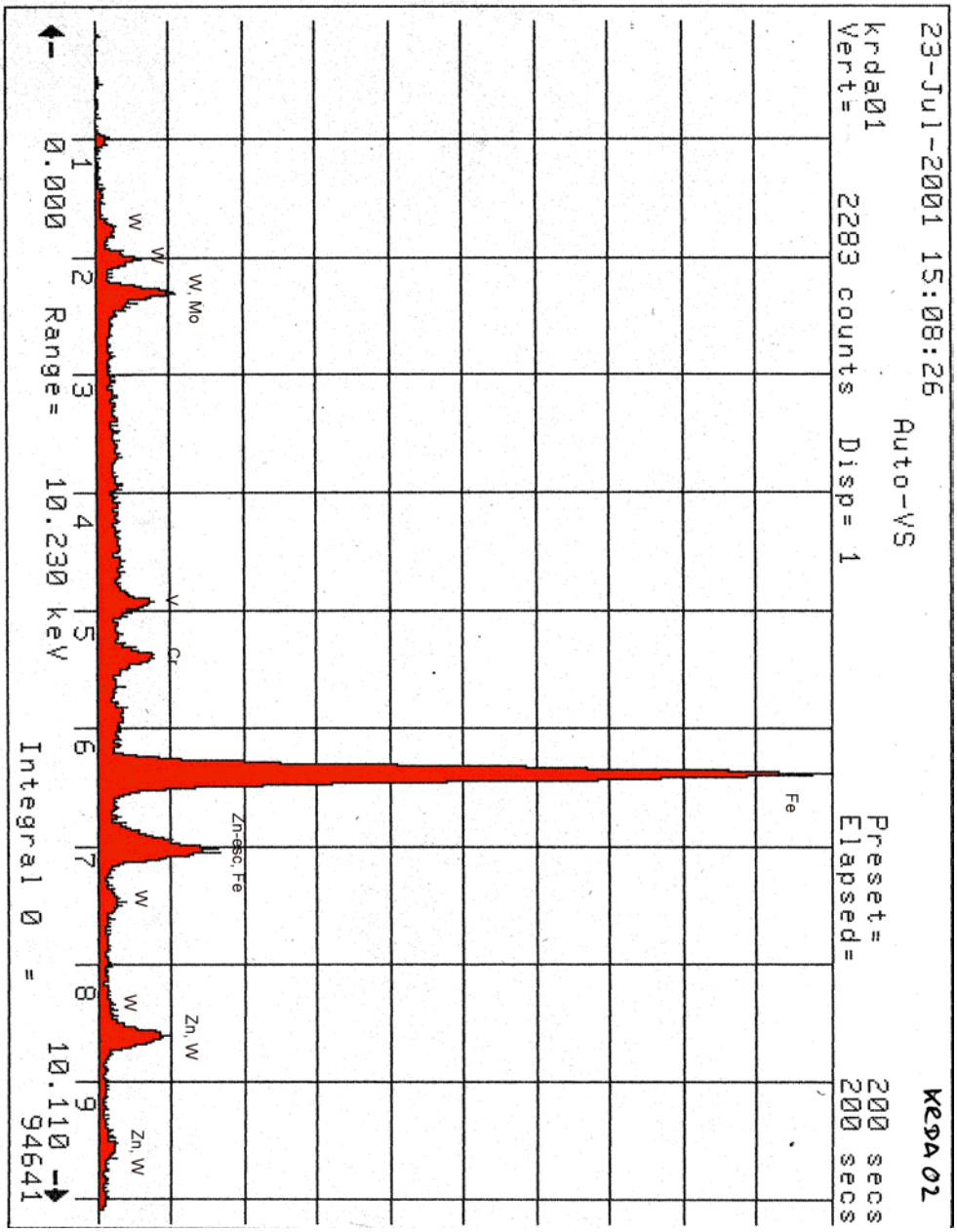
23-Jul-2001 15:08:26
Auto-VS
KRDA 02
krda01
Vert= 2283 counts Disp= 1
Preset= 200 secs
Elapsed= 200 secs
Fe
W
W
W, Mo
V
Cr
Zn-esc. Fe
W
W
Zn, W
Zn, W
0.000
Range= 10.230 keV
Integral 0 = 10.110
94641

KRDA 03

23-Jul-1901 15:18:20 krda01

Accelerating voltage	20.0 KeV
Beam - sample incidence angle	90.0 degrees
Xray emergence angle	17.1 degrees
Xray - window incidence angle	0.1 degrees

STANDARDLESS EDS ANALYSIS
(XPP QUANTITATION)

ELEMENT & LINE	WEIGHT PERCENT	ATOMIC PERCENT*	PRECISION 2 SIGMA	COMPUTED K-RATIO**
V KA	3.11	3.76	0.11	0.0302
Cr KA	4.75	5.64	0.13	0.0506
Fe KA	71.88	79.47	0.61	0.7014
Zn KA	4.32	4.08	0.23	0.0372
Mo LA	5.48	3.53	0.24	0.0322
W LA	10.45	3.51	0.65	0.0764
TOTAL	100.00			

ITERATIONS 6

*NOTE: ATOMIC PERCENT is normalized to 100

**NOTE: K-RATIO = K-RATIO x R
where R = reference(standard)/reference(sample)

NORMALIZATION FACTOR: 1.000

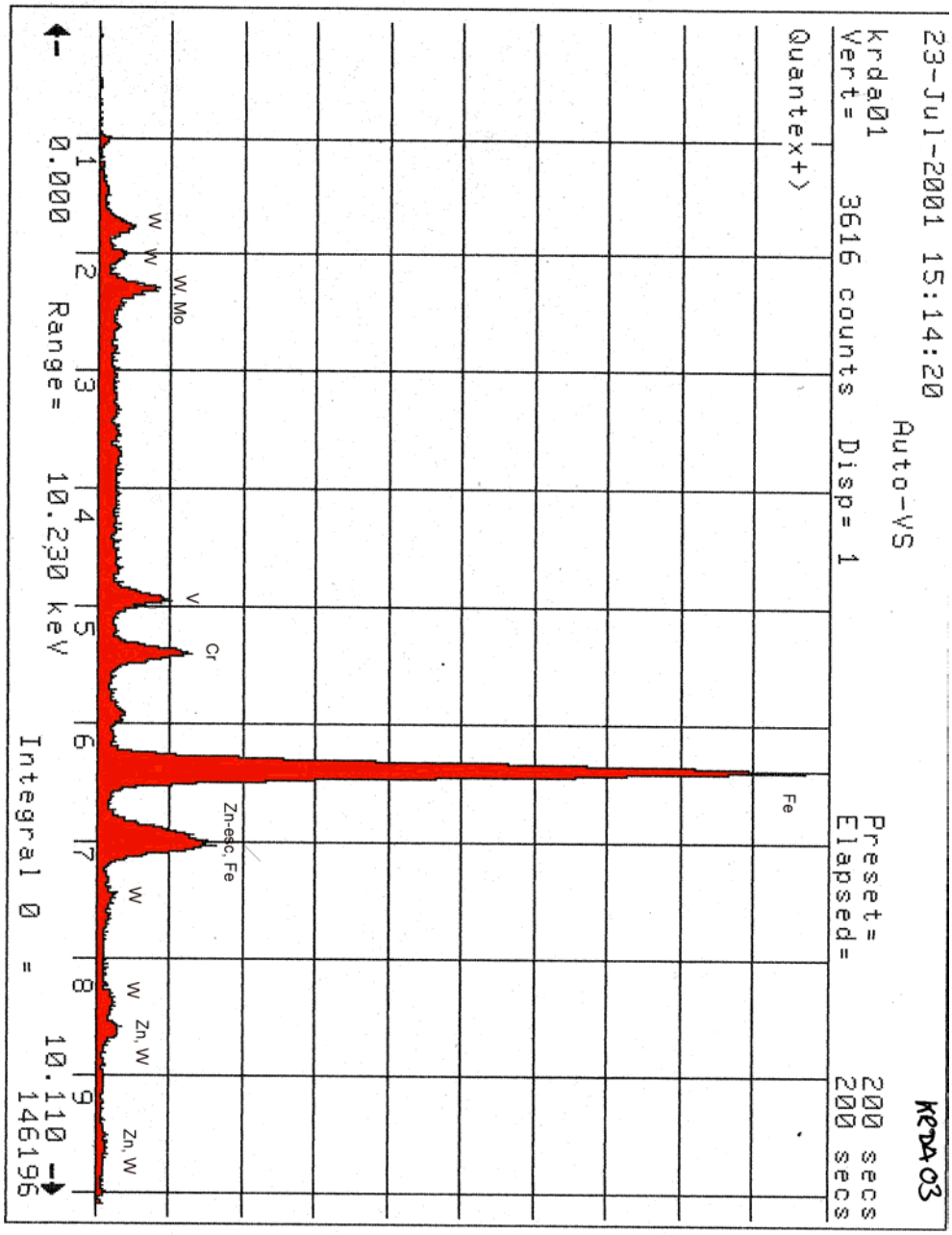
23-Jul-2001 15:14:20
Auto-VS
KRDA03
krda01
Vert= 3616 counts Disp= 1
Preset= 200 secs
Elapsed= 200 secs
Quantex+)
Fe
Zn-esc, Fe
Cr
V
W, Mo
W
Zn, W
0.000
Range= 10.230 keV
10.110
Integral 0 = 146196

KRDA04

23-Jul-1901 15:33:35 krda04

Accelerating voltage	20.0 KeV
Beam - sample incidence angle	90.0 degrees
Xray emergence angle	17.1 degrees
Xray - window incidence angle	0.1 degrees

STANDARDLESS EDS ANALYSIS
(XPP QUANTITATION)

ELEMENT & LINE	WEIGHT PERCENT	ATOMIC PERCENT*	PRECISION 2 SIGMA	COMPUTED K-RATIO**
V KA	1.95	2.47	0.11	0.0182
Cr KA	2.19	2.72	0.12	0.0223
Fe KA	55.25	63.83	0.68	0.5460
Zn KA	19.07	18.83	0.59	0.1703
Mo LA	14.31	9.62	0.48	0.0854
W LA	7.23	2.54	0.67	0.0549
TOTAL	100.00			

ITERATIONS 6

*NOTE: ATOMIC PERCENT is normalized to 100

**NOTE: K-RATIO = K-RATIO x R
where R = reference(standard)/reference(sample)

NORMALIZATION FACTOR: 1.000

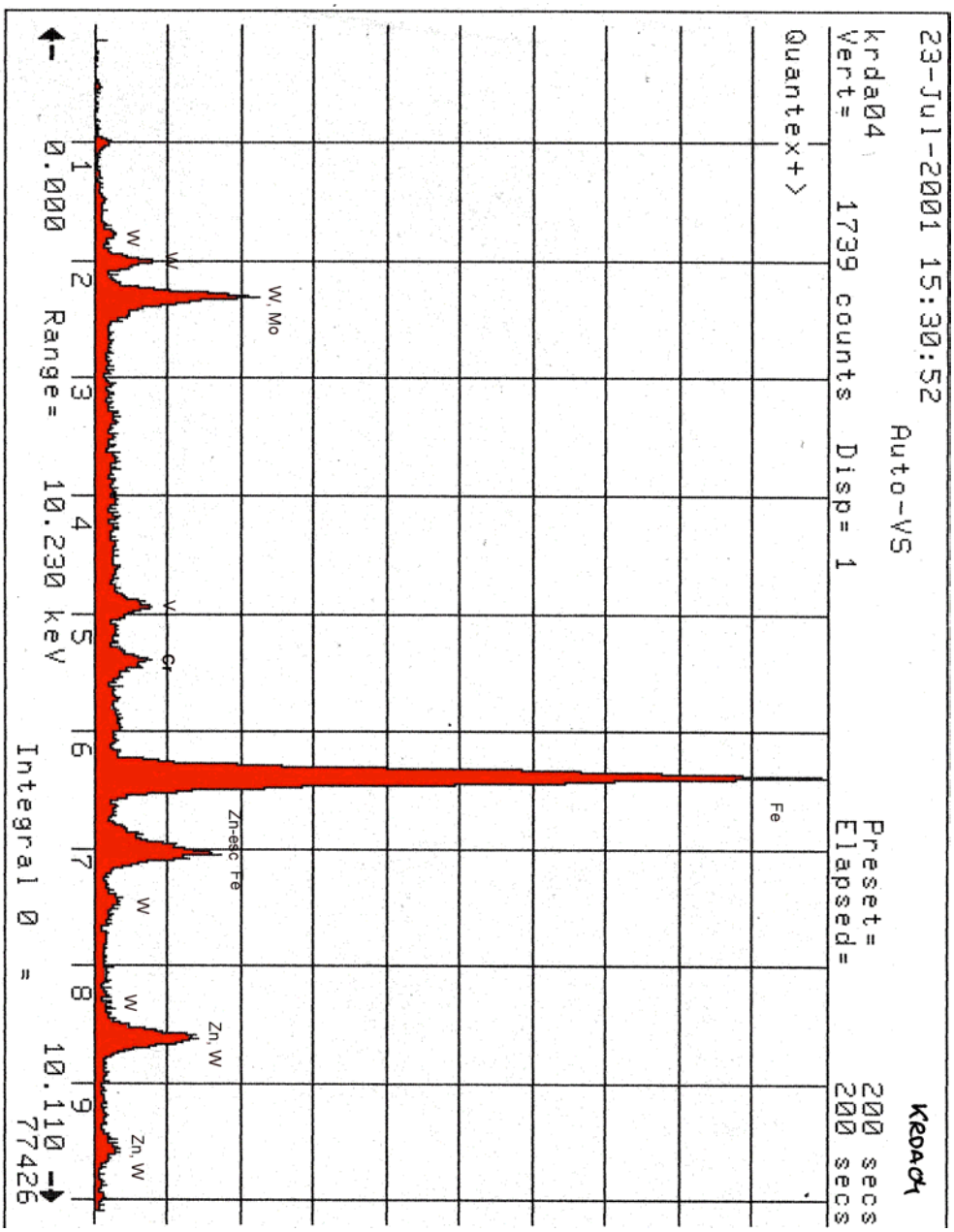
23-Jul-2001 15:30:52
Auto-VS
KRDA04
krda04
Vert= 1739 counts Disp= 1
Preset= 200 secs
Elapsed= 200 secs
Quantex+>
Fe
W
W
W, Mo
V
Cr
Zn-esc Fe
W
W
Zn, W
Zn, W
0.000
Range= 10.230 keV
Integral 0 = 10.110
77426

8 List of references

1. Petersen, T.Ø., Cyclic Plasticity and Low Cycle Fatigue in Tool Materials, Ph.D.-Thesis, Technical University of Denmark, Department of Solid Mechanics, 1998.
2. Brøndsted, P.; Skov-Hansen, P., Int. J. Fatigue, 1998, Vol. 20, No. 5, pp. 373-381.
3. Skov-Hansen, P.; Bay, N.; Grønbæk, J.; Brøndsted, P., Journal of Materials Processing Technology. 1999, 95 (1-3), pp. 40-48.
4. Nielsen, E.B.; Grønbæk, J., Journal of Materials Processing Technology. 2000, 98 (2), pp. 155-161.
5. Roberts, G.; Krauss, G.; Kennedy, R., Tool Steels, 5th. Edition, ASM International, 1998.
6. Davis, J.R. ASM specialty handbook, Tool Materials, ASM International, 1995.
7. Højerslev, C., Tool Steels, Risø-R-1244(EN), Risø National Laboratory, Roskilde, Denmark, 2001.
8. Hwang, K.C.; Lee, S.; Lee, H.C., Materials Science & Engineering A254, 1998, pp 282-295.
9. Højerslev, C.; Carstensen, J.V.; Brøndsted, P.; Somers, M.A.J., "Fracture Crack Behaviour in a High Strength Tool Steel", In: Proceedings of the 8th International Fatigue Congress- "FATIGUE 2002", June 2-7, 2002, Stockholm, Sweden, Vol. 5.
10. Anderson, J.C.; Leaver, K.D.; Rawlings, R.D.; Alexander, J.M., Materials Science – Third Edition, Van Nostrand Reinhold (UK) Co. Ltd. 1985.
11. Metals Handbook®, Ninth Edition, Vol. 12, "Fractography".
12. C. Brundle, R.; Evans Jr., C.A.; Wilson, S., Encyclopaedia of Materials Characterization, Butterworth-Heinemann, USA, 1992.
13. Goodhew, P.J.; Humphreys, F.J., Electron Microscopy and Analysis, 2nd ed., Taylor & Francis 1997.
14. Eberhart J.P., Structural and Chemical Analysis of Materials, John Wiley & Sons 1991.
15. Krupp Presta AG 1.st year report.

Title and authors

Fractography analysis of tool samples used for cold forging

Kristian Vinter Dahl

ISBN	ISSN
87-550-3102-1; 87-550-3104-8 (Internet)	0106-2840

Department or group	Date
Materials Research Department	August 2002

Groups own reg. number(s)	Project/contract No(s)

Sponsorship

Pages	Tables	Illustrations	References
52	5	42	15

Abstract (max. 2000 characters)

Three fractured tool dies used for industrial cold forging have been investigated using light optical microscopy and scanning electron microscopy. Two of the specimens were produced using the traditional Böhler P/M steel grade s790, while the last specimen was a third generation P/M steel produced using new technology developed by Böhler. All three steels have the same nominal composition of alloying elements.

The failure in both types of material occurs as a crack formation at a notch inside of the tool. Generally the cold forging dies constructed in third generation steels have a longer lifetime than the ones constructed in traditional steel, which is connected to differences in micro-structure. Focus has been put on differences in the size and distribution of carbides. It is found that the third generation steel contains smaller and more finely dispersed carbides and has an increased resistance towards abrasive wear compared with the traditional P/M steel.

It was discovered that a cleaning agent (Alconox) frequently used for the cleaning of fracture surfaces introduced changes to the surface morphology. Therefore work was put into finding out exactly how this influenced the specimens looked upon. The result of this work is in-cluded as a separate part of this document (Appendix A).

Descriptors INIS/EDB

Available on request from Information Service Department, Risø National Laboratory,
(Afdelingen for Informationsservice, Forskningscenter Risø), P.O.Box 49, DK-4000 Roskilde, Denmark.
Telephone +45 4677 4004, Telefax +45 4677 4013